



# A comparison study between CMAQ-simulated and OMI-retrieved NO<sub>2</sub> columns over East Asia for evaluation of NO<sub>x</sub> emission fluxes of INTEX-B, CAPSS, and REAS inventories

K. M. Han<sup>1,2</sup>, S. Lee<sup>1,2</sup>, L. S. Chang<sup>3</sup>, and C. H. Song<sup>1,2</sup>

<sup>1</sup>School of Environmental Science and Engineering, Gwangju Institute of Science and Technology (GIST), Gwangju, South Korea

<sup>2</sup>Advanced Environmental Monitoring Research Center (ADEMRC), Gwangju Institute of Science and Technology (GIST), Gwangju, 500-712, South Korea

<sup>3</sup>Air Quality Monitoring and Forecasting Center, National Institute of Environmental Research (NIER), Incheon, 404-708, South Korea

Correspondence to: C. H. Song (chsong@gist.ac.kr)

Received: 17 June 2014 – Published in Atmos. Chem. Phys. Discuss.: 30 June 2014

Revised: 17 December 2014 – Accepted: 12 January 2015 – Published: 24 February 2015

**Abstract.** Comparison between the CMAQ (Community Multi-scale Air Quality Model)-calculated and OMI (Ozone Monitoring Instrument)-retrieved tropospheric NO<sub>2</sub> columns was carried out for 2006 over East Asia (100–150° E; 20–50° N) to evaluate the bottom-up NO<sub>x</sub> emission fluxes of INTEX-B, CAPSS, and REAS v1.11 inventories. The three emission inventories were applied to the CMAQ model simulations for the countries of China, South Korea, and Japan, respectively. For the direct comparison between the two NO<sub>2</sub> columns, the averaging kernels (AKs) obtained from the Royal Netherlands Meteorological Institute (KNMI)/DOMINO v2.0 daily product were applied to the CMAQ-simulated data. The analysis showed that the two tropospheric NO<sub>2</sub> columns from the CMAQ model simulations and OMI observations ( $\Omega_{\text{CMAQ,AK}}$  and  $\Omega_{\text{OMI}}$ ) had good spatial and seasonal correlation, with correlation coefficients ranging from 0.71 to 0.96. In addition, the normalized mean errors (NMEs) between the  $\Omega_{\text{CMAQ,AK}}$  and  $\Omega_{\text{OMI}}$  were found to range from ~40 to ~63%. The  $\Omega_{\text{CMAQ,AK}}$  were, on annual average, ~28% smaller (in terms of the NMEs) than the  $\Omega_{\text{OMI}}$ , indicating that the NO<sub>x</sub> emissions used were possibly underestimated in East Asia. Large absolute differences between the  $\Omega_{\text{CMAQ,AK}}$  and  $\Omega_{\text{OMI}}$  were found, particularly over central eastern China (CEC) during winter (annual averaged mean error of  $\sim 4.51 \times 10^{15}$  molecules cm<sup>-2</sup>). Although such differences between the  $\Omega_{\text{CMAQ,AK}}$  and  $\Omega_{\text{OMI}}$  are likely caused by the errors and biases in the NO<sub>x</sub> emis-

sions used in the CMAQ model simulations, it can be rather difficult to quantitatively relate the differences to the accuracy of the NO<sub>x</sub> emissions, because there are also several uncertain factors in the CMAQ model, satellite-retrieved NO<sub>2</sub> columns and AK products, and NO<sub>x</sub> and other trace gas emissions. In this context, three uncertain factors were selected and analyzed with sensitivity runs (monthly variations in NO<sub>x</sub> emissions; influences of different NO<sub>x</sub> emission fluxes; and reaction probability of N<sub>2</sub>O<sub>5</sub> radicals). Other uncertain or possible influential factors were also discussed to suggest future direction of the study.

## 1 Introduction

There has been growing public concern about serious smog events in East Asia due to large amounts of anthropogenic pollutants in the atmosphere. Among the pollutants, nitrogen oxides (NO<sub>x</sub>  $\cong$  NO + NO<sub>2</sub>) play a key role in tropospheric chemistry, such as ozone and secondary aerosol formation. Also, in global climate change, atmospheric NO<sub>x</sub> is believed to make indirect negative contributions to radiative forcing in the atmosphere (Wild et al., 2001). For example, secondary nitrates (NO<sub>3</sub><sup>-</sup>) formed via the condensation of atmospheric HNO<sub>3</sub>, NO<sub>3</sub>, and N<sub>2</sub>O<sub>5</sub> into particles contribute, on average, 30.7% to aerosol direct radiative forcing (ADRF) in East

Asia during the winter season, which cannot be ignored in the estimation of direct radiative forcing in East Asia (Park et al., 2014). HNO<sub>3</sub> formation via the reaction of OH + NO<sub>2</sub> during the daytime and heterogeneous nitrate formation via the condensation of N<sub>2</sub>O<sub>5</sub> onto atmospheric particles during the nighttime are believed to be the main chemical and physicochemical processes removing NO<sub>x</sub> from the atmosphere (McConnell and McElroy, 1973; Platt et al., 1984; Dentener and Crutzen, 1993; Brown et al., 2006; Han and Song, 2012).

Recently, several studies have reported annual increases in NO<sub>x</sub> emissions in China (Zhang et al., 2007, 2009; Kurokawa et al., 2013). For example, according to the Greenhouse gas and Air Pollution Interactions and Synergies (GAINS) model simulations, China makes the largest contribution to global NO<sub>x</sub> emissions, and its contribution was estimated to be 25 % for 2010 (Cofala et al., 2012). Also, when several emissions scenarios are applied to the GAINS simulations, the contribution of China is estimated to increase, to ~29 % in the years between 2015 and 2035 (Cofala et al., 2012). However, large uncertainty in bottom-up NO<sub>x</sub> emissions over East Asia has been reported (e.g., Streets et al., 2003; Zhang et al., 2007; Klimont et al., 2009; Xing et al., 2011).

In the meantime, several studies have also reported rapid increases in atmospheric NO<sub>2</sub> columns over China, based on Global Ozone Monitoring Experiment (GOME), Ozone Monitoring Instrument (OMI), and SCanning Imaging Absorption spectroMeter for Atmospheric CHartography (SCIAMACHY) observations (Richter et al., 2005; van der A et al., 2006; Schneider and van der A, 2012; Hilboll et al., 2013; Itahashi et al., 2014). These satellite observations have provided useful global/regional information on the spatial distributions of NO<sub>2</sub> columns, and have also been used to investigate the accuracy of the global and regional NO<sub>x</sub> emissions (e.g., Martin et al., 2006; Uno et al., 2007; Wang et al., 2007; Han et al., 2009).

However, these satellite observations are not “real” or “true” values, having different vertical sensitivities at different altitudes in the atmosphere. To consider this vertical sensitivity of the satellite observations, averaging kernels (AKs) should be introduced into comparison studies between chemistry-transport model (CTM)-simulated and satellite-retrieved tropospheric NO<sub>2</sub> columns (hereafter, denoted as  $\Omega$ ). The introduction of AKs could correct the large systematic errors typically caused by assumed (or unrealistic) NO<sub>2</sub> vertical profiles used in the retrieval process of the NO<sub>2</sub> columns (Rodgers, 2000; Eskes and Boersma, 2003). In particular, Eskes and Boersma (2003) reported that the use of AKs is crucial in interpreting the retrieved  $\Omega$ , because of the low sensitivity of satellite observations of NO<sub>2</sub> near the surface areas.

In this context, several studies have used AKs to evaluate the surface NO<sub>x</sub> emissions over several regions (e.g., Herron-Thorpe et al., 2010; Lamsal et al., 2010; Huijnen et al., 2010; Ghude et al., 2013; Zyrichidou et al., 2013). The

previous studies conducted by Han et al. (2009, 2011) also compared the CTM-calculated tropospheric NO<sub>2</sub> columns with GOME-retrieved tropospheric NO<sub>2</sub> columns to evaluate the bottom-up NO<sub>x</sub> emissions over East Asia, but without using the AKs. Based on the comparison, Han et al. (2011) concluded that the bottom-up NO<sub>x</sub> emissions used in CTM simulations over East Asia may be overestimated. However, such a comparison without the application of AKs is like comparing apples with oranges, and is unreasonable. Therefore, one of the main objectives of this study was to correct our previous conclusions, using the state-of-the-science knowledge and methods, including the application of AKs to the CTM simulations. In this study, we intended to evaluate three bottom-up NO<sub>x</sub> emissions of INTEX-B, CAPSS, and REAS v1.11 inventories in East Asia, using OMI-retrieved tropospheric NO<sub>2</sub> columns ( $\Omega_{\text{OMI}}$ ) from KNMI/DOMINO v2.0 daily products and the CTM-calculated tropospheric NO<sub>2</sub> columns ( $\Omega_{\text{CTM}}$ ). To conduct this investigation, the AKs obtained from the KNMI algorithm were applied, and then direct comparison of the  $\Omega_{\text{CTM,AK}}$  with  $\Omega_{\text{OMI}}$  was carried out (refer to Sect. 3.1).

However, evaluation of the bottom-up NO<sub>x</sub> emissions via comparison between  $\Omega_{\text{CTM,AK}}$  and  $\Omega_{\text{OMI}}$  may be hampered by many uncertain factors such as (i) uncertain temporal variations in NO<sub>x</sub> emissions in East Asia; (ii) uncertainty in meteorological fields; (iii) uncertain or missing photochemistries in the CTM; and (iv) errors in the retrieved NO<sub>2</sub> columns and AKs. Because of these errors and uncertainties, it can sometimes be difficult to directly and quantitatively relate the differences between the  $\Omega_{\text{CMAQ,AK}}$  and  $\Omega_{\text{OMI}}$  to the accuracy of the NO<sub>x</sub> emissions in East Asia. Some of these issues are therefore explored with several sensitivity analyses, and other factors are also discussed in Sect. 3.2.

## 2 Experimental methods

### 2.1 Modeling descriptions

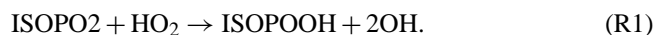
First, for the CTM simulations, the US EPA/Models-3 CMAQ (Community Multi-scale Air Quality) v4.7.1 model was used (Byun and Schere, 2006). To drive CMAQ model simulations, two main drivers are needed: (i) meteorological fields and (ii) emission fields. For the former, PSU/NCAR MM5 (Pennsylvania State University/National Center for Atmospheric Research Mesoscale Model 5) v3.7.1 was used with National Centers for Environmental Prediction (NCEP) reanalyzed data sets (Stauffer and Seaman, 1990, 1994). To prepare more accurate meteorological fields, four-dimensional data assimilation (FDDA) using QuickSCAT 10 m wind data sets was also carried out. For the latter, three anthropogenic emission inventories were used: INTEX-B (Intercontinental Chemical Transport Experiment-Phase B, Zhang et al., 2009), CAPSS (Clean Air Policy Support System, Hong et al., 2008), and REAS v1.11 (Regional Emis-

sion Inventory in Asia, Ohara et al., 2007) emission inventories for the year 2006. Annual  $0.5^\circ \times 0.5^\circ$ -resolved INTEX-B and REAS v1.11 emissions were interpolated into the CMAQ grid cells in China and Japan, respectively. For biogenic emissions, the MEGAN-ECMWF (Model of Emissions of Gases and Aerosols from Nature–European Center for Medium-Range Weather Forecasts) inventory was obtained from the official website, at <http://tropo.aeronomie.be/models/isoprene.htm> (Müller et al., 2008). Biogenic emissions are an important factor during the summer, even in this type of NO<sub>x</sub> study, because the mixing ratios of biogenic species can influence the NO<sub>2</sub>-to-NO ratios via changing the levels of HO<sub>x</sub> and RO<sub>2</sub> radicals (Horowitz et al., 2007; Han et al., 2009). The accuracy of the biogenic emissions used in this study was also evaluated over the same domain, East Asia, as in our previous study (Han et al., 2013).

Table 1 summarizes the base-case simulation and several sensitivity runs for this study. For the base-case simulation, monthly variations of the anthropogenic NO<sub>x</sub> emissions from Zhang et al. (2009) were considered for China, while those from Han et al. (2009) were used for South Korea and Japan. The monthly factors were applied to the sectors of power generation, residential areas, industry, and transportation. As shown in Fig. 1, data on several monthly variations in NO<sub>x</sub> emissions over China were available. Among them, two representative and extreme monthly variations were chosen in this study, which were explored and discussed in Sect. 3.2.1.

The modeling period was from 1 January to 31 December 2006. In this study, 2006 was chosen because the INTEX-B inventory was compiled for this year (the REAS v1.11 and CAPSS inventories were also chosen for 2006). The horizontal domain covers from 100 to 150° E and from 20 to 50° N with a grid-resolution of 30 km × 30 km. The vertical domain covers from 1000 to 118 hPa with 14 terrain following  $\sigma$ -coordinates. For considering aerosol dynamics and thermodynamics, the aerosol module of AERO4 was selected (Binkowski and Roselle, 2003).

For the consideration of gas-phase chemistry, the SAPRAC-99 (Statewide Air Pollution Research Center-99) mechanism was selected (Carter, 2000). Then, to consider unknown OH radical processes (Lelieveld et al., 2008), the SAPRAC-99 mechanism was modified partly, based on the work of Butler et al. (2008) in the following way. See Reaction (R1):



Here, ISOPO<sub>2</sub> and ISOPOOH represent isoprene-derived peroxy radical and peroxide, respectively. Other schemes used in the CMAQ model simulations were the global mass-conserving scheme (YAMO) for horizontal and vertical advection (Yamartino, 1993), the asymmetric convective model (ACM) algorithm for convective cloud mixing, and ACM (ver. 2) for vertical diffusion (Pleim, 2007).

In the CMAQ modeling, initial conditions (ICs) were prepared from 1 week-long spin-up model simulations, and

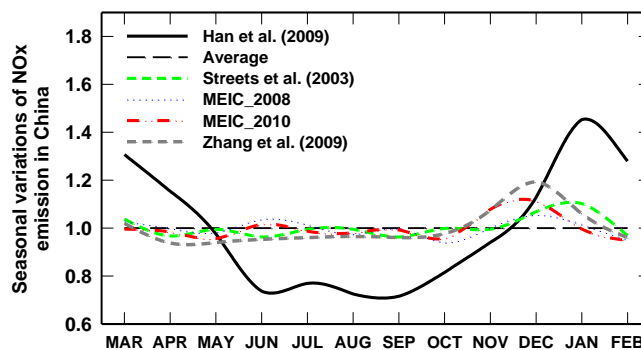


**Figure 1.** Monthly variation in NO<sub>x</sub> emissions in China. Here, the “MEIC\_2008” and “MEIC\_2010” were obtained from the website, <http://www.meicmodel.org/>.

boundary conditions (BCs) were obtained from global CTM simulations, MOZART (Model for OZone And Related chemical Tracers) (Emmons et al., 2010). The MOZART model simulation data for the BCs were obtained from <http://www.acd.ucar.edu/wrf-chem/mozart.shtml>. Other details about the model setup were reported by Han et al. (2013).

For synchronization with the  $\Omega_{\text{OMI}}$ , the  $\Omega_{\text{CMAQ}}$  data were collected and then averaged between 13:00 and 14:00 local time (LT), because the OMI sensor scans the atmosphere over East Asia approximately at 13:45 LT. For further detailed analyses, eight highly populated focus regions were defined in this study, and are presented in Fig. 2.

## 2.2 OMI-retrieved NO<sub>2</sub> columns and AKs

The OMI instrument on board the NASA/EOS–Aura satellite, a nadir-viewing imaging spectrometer, provides information on the properties of aerosols and clouds as well as global levels of atmospheric species such as ozone, NO<sub>2</sub>, SO<sub>2</sub>, OClO, BrO, and HCHO on a daily basis via observing backscattered UV-VIS radiances from 270 to 550 nm (Levelt et al., 2006). Two-dimensional charge-coupled device (CCD) detectors equipped in the OMI instrument observe the atmosphere with a spatial resolution of 13 km × 24 km at the nadir. CCD1 covers the UV channel of 270–310 nm and 310–365 nm. The visible channel, ranging from 365 to 500 nm, is covered by CCD2 to observe NO<sub>2</sub>.

In this study, daily levels of OMI-retrieved tropospheric NO<sub>2</sub> columns from KNMI/DOMINO v2.0 products were used (Boersma et al., 2007, 2011a). The KNMI/DOMINO v2.0 algorithm (hereafter, KNMI algorithm) for retrieving the tropospheric NO<sub>2</sub> columns from the OMI radiance data proceeds in the following sequence. First, a slant NO<sub>2</sub> column density was determined from spectral fitting, using the differential optical absorption spectroscopy (DOAS) method. Second, the stratospheric NO<sub>2</sub> contribution was removed by subtracting the stratospheric portions of slant NO<sub>2</sub> columns from the total slant NO<sub>2</sub> columns. The stratospheric NO<sub>2</sub>

**Table 1.** Description of CMAQ model simulations conducted in this study.

Cases	Sensitivity test	Month, Year	Description	Section
1	Base-case simulation	Jan–Dec 2006	Seasonal variation of NO <sub>x</sub> emission from INTEX-B inventory for China (Zhang et al., 2009) and from Han et al. (2009) for South Korea and Japan. NO <sub>x</sub> emissions from INTEX-B, CAPSS, and REAS inventories for China, South Korea, and Japan, respectively Parameterization of $\gamma_{\text{N}_2\text{O}_5}$ from the combination of Riemer et al. (2003) and Evans and Jacob (2005)	Sect. 3.1
2	Seasonal variation of NO <sub>x</sub> emission	Jan–Dec 2006	As case 1 except for seasonal variation of NO <sub>x</sub> emission from Han et al. (2009) for China (i.e., all the monthly factors from Han et al. (2009) for China, South Korea, and Japan.)	Sect. 3.2.1
3	Emission strength	Jan 2006	As case 1 except for NO <sub>x</sub> emissions from REAS inventory for China	Sect. 3.2.2
4	Reaction probability of N <sub>2</sub> O <sub>5</sub>	Jan 2006	As case 1 except for the $\gamma_{\text{N}_2\text{O}_5}$ parameterizations from: (i) Dentener and Crutzen (1993); (ii) Riemer et al. (2003); (iii) Davis et al. (2008); and (iv) Brown et al. (2006)	Sect. 3.2.3

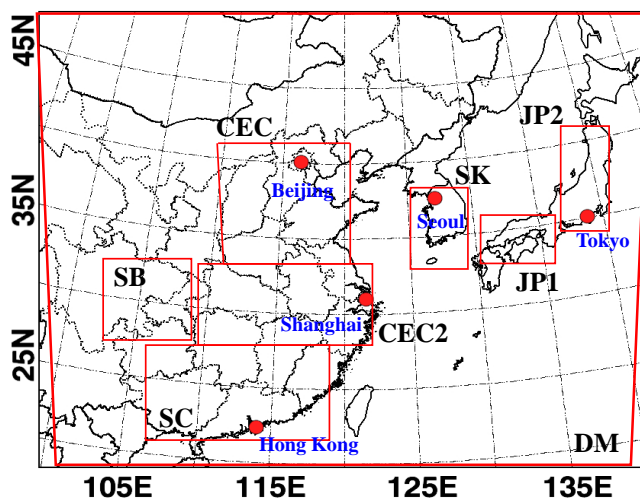
slant columns were calculated by data assimilation of OMI-observed slant NO<sub>2</sub> columns in the global CTM (TM4) (Boersma et al., 2007). Finally, the tropospheric slant NO<sub>2</sub> columns were converted into vertical NO<sub>2</sub> columns, using the air mass factor (AMF), defined as the ratio of the measured slant column to the vertical column. This AMF is a function of several factors, such as the satellite viewing geometry, surface albedo, surface pressure, and vertical distributions of clouds, aerosols, and trace gases.

In this study, to reduce retrieval errors, measured scenes with surface albedo values larger than 0.3 were excluded, as suggested by Boersma et al. (2011b). The surface albedo data was obtained from the OMI observations (Kleipool et al., 2008). Also, observed pixels with cloud radiance fractions (CRFs) larger than 50 % were filtered out, which are approximately equivalent to cloud fractions (CFs) smaller than 20 % (van der A et al., 2006). Thus, OMI-retrieved tropospheric NO<sub>2</sub> columns under almost “cloud-free” conditions were used in this study.

Errors in the retrieval of the  $\Omega_{\text{OMI}}$  can mainly be caused by calculations of the AMFs. Boersma et al. (2011a) reported that errors of the  $\Omega_{\text{OMI}}$  mostly due to calculations of the AMFs in KNMI/DOMINO v2.0 products were approximated to be  $\sim 1.0 \times 10^{15}$  molecules cm<sup>-2</sup>, with a relative error of 25 %. The other errors in the products were from the spectral fitting ( $\sim 0.7 \times 10^{15}$  molecules cm<sup>-2</sup>) and the stratospheric slant column ( $\sim 0.25 \times 10^{15}$  molecules cm<sup>-2</sup>).

The AKs were also applied to the CMAQ model simulations. The AKs are analytically expressed in Eq. (1) (Rodgers, 2000; Eskes and Boersma, 2003):

$$\begin{aligned}
 \text{AK} &= G_y K_x \\
 &= \frac{\partial R}{\partial y} \frac{\partial F}{\partial x} \\
 &= \frac{\partial \hat{x}}{\partial x},
 \end{aligned}
 \quad (1)$$

**Figure 2.** Study domain and eight focus regions in this study: central eastern China (CEC), central eastern China 2 (CEC2), southern China (SC), Sichuan Basin (SB), South Korea (SK), western part of Japan (JP1), eastern part of Japan (JP2), and the entire domain (DM).

where  $G_y$  and  $K_x$  represent the sensitivities of the retrieval ( $R$ ) to the measurement ( $y$ ) and the forward model ( $F$ ) to the state ( $x$ ), respectively. Also,  $K_x$  is known as a weighting function or Jacobian matrix. Thus, as shown in Eq. (1), the AKs represent the sensitivity of the retrieved quantities (here, vertical NO<sub>2</sub> column,  $\hat{x}$ ) to the true atmospheric state ( $x$ ). Using the AKs, the retrieved quantity ( $\hat{x}$ ) can be expressed by Eq. (2):

$$\hat{x} - \hat{x}_a = \text{AK}(x - x_a) + \varepsilon, \quad (2)$$

where  $x_a$  and  $\varepsilon$  represent a priori estimate and total error in measured signal relative to the forward model, respectively. Information on the AKs and retrieved quantity are

included in the daily KNMI products ([http://www.temis.nl/airpollution/no2col/no2regioomi\\_v2.php](http://www.temis.nl/airpollution/no2col/no2regioomi_v2.php)).

Figure 3 presents the vertical distributions of the seasonally averaged AKs retrieved from the KNMI algorithms over Central East China (CEC) and other regions (defined in Fig. 2). As shown in Fig. 3, the AKs are strongly altitude-dependent in the troposphere. For example, near the surface, the AKs are smaller than unity, ranging between 0.2 and 0.7 (based on seasonal averaged values). In contrast, in the upper troposphere, the AKs are larger than unity, ranging between 1.1 and 2.1 (an AK of unity means that the OMI instruments can directly measure the true NO<sub>2</sub> column densities). Additionally, the AKs are generally lower in warm seasons than in cold seasons. These low values in the AKs during the summer are probably related to low surface albedos, low concentrations of aerosols, and large uncertainty in cloud retrieval during the summer (Eskes and Boersma, 2003).

Figure 4 illustrates the main procedures of the comparison study. Once the CMAQ model simulations were done, all the vertically resolved NO<sub>2</sub> mixing ratios were interpolated to the OMI footprints on a daily basis since the AKs are defined for the OMI footprints. Interpolating AKs to model grid cells is not recommended because the AKs are sometimes sensitive to changes on small spatial scales (Boersma et al., 2011b). After this, the AKs under almost cloud-free conditions were applied to the NO<sub>2</sub> mixing ratios at different layers, and were then integrated from surface to tropopause in order to calculate  $\Omega_{\text{CMAQ,AK}}$ . Meanwhile, the tropospheric NO<sub>2</sub> columns were retrieved from the OMI observations via the KNMI algorithms. A direct comparison study was then made between the two  $\Omega$  products (i.e.,  $\Omega_{\text{OMI}}$  vs.  $\Omega_{\text{CMAQ,AK}}$ ).

For the purpose of this study, the seasonal average values of  $\Omega_{\text{OMI}}$  and  $\Omega_{\text{CMAQ,AK}}$  were calculated (in case of the  $\Omega_{\text{CMAQ,AK}}$ , daily AK applications were first conducted and then seasonal average values were calculated). Seasonal averaging was carried out to reduce the “random errors” in the NO<sub>2</sub> retrieval process typically caused by instrument signal noise, fitting errors, and uncertainty in cloud information. It has been suggested and demonstrated that the random errors can be reduced by both temporal and/or spatial averaging (Fioletov et al., 2002; Monaghan et al., 2006; Johnson et al., 2007; Richter et al., 2011; Clarisse et al., 2013).

On the other hand, the application of AKs can reduce “smoothing errors” in the NO<sub>2</sub> retrieval process, which are mainly caused by bias in the a priori vertical NO<sub>2</sub> profiles. As mentioned previously, TM4-derived a priori profiles were used in the OMI NO<sub>2</sub> retrieval process, which can sometimes cause serious smoothing errors. In order to correct such errors, AKs were applied to the CMAQ model simulations in this study (Rodgers, 2000; Eskes and Boersma, 2003). After the application of AKs, a priori information from TM4 did not influence the comparison between  $\Omega_{\text{OMI}}$  and  $\Omega_{\text{CMAQ,AK}}$ .

### 3 Results and discussions

The objective of this study is to evaluate the NO<sub>x</sub> emissions of the INTEX-B, CAPSS, and REAS v1.11 inventories over East Asia by comparing two  $\Omega$  obtained from the CMAQ model simulations and OMI observations (Sect. 3.1). In addition, several sensitivity analyses were also conducted to examine the influences of the uncertainty factors on the discrepancies between  $\Omega_{\text{CMAQ,AK}}$  and  $\Omega_{\text{OMI}}$  (Sect. 3.2). Obviously, not all the influential factors can be explored within the framework of this study. Thus, several selected issues that may be important are also discussed further in Sect. 3.2.4.

#### 3.1 Comparison between CMAQ-estimated and OMI-retrieved NO<sub>2</sub> columns: Case 1

##### 3.1.1 CMAQ-calculated vs. OMI-retrieved NO<sub>2</sub> columns

In this study, the analyses were conducted for four seasons: (i) spring (March–May 2006), (ii) summer (June–August 2006), (iii) fall (September–November 2006), and (iv) winter (January–February 2006 and December 2006). For more detailed analyses, eight focus regions were also defined: (i) central eastern China (CEC), (ii) central eastern China 2 (CEC2), (iii) southern China (SC), (iv) Sichuan Basin (SB), (v) South Korea (SK), (vi) the western part of Japan (JP1), (vii) the eastern part of Japan (JP2), and (viii) the entire domain (DM) (refer to Fig. 2 regarding the domains).

Figure 5 presents the comparison analysis between the  $\Omega_{\text{CMAQ}}$  and  $\Omega_{\text{OMI}}$  for the four seasons over East Asia before and after the applications of the AKs. As shown in Fig. 5, the CMAQ model simulations (the first and second columns) show spatially and seasonally consistent patterns with OMI observations (the third column). For example, the high values of the  $\Omega_{\text{OMI}}$  over the densely populated and economically developed megacity regions such as Beijing, Shanghai, Hong Kong, Seoul, and Tokyo (refer to Fig. 2 regarding their locations) are well captured by the CMAQ model simulations. The levels of the  $\Omega$  during the winter are distinctly high. Also, the low values of the  $\Omega_{\text{CMAQ}}$  during the summer are well matched with those from the OMI observations. The low levels of the  $\Omega$  during the summer are mainly caused by active NO<sub>x</sub> chemical losses via the reaction of NO<sub>2</sub> with OH radicals (McConnell and McElroy, 1973; Atkinson et al., 2004; Boersma et al., 2009; Han et al., 2009; Stavrou et al., 2013). The uncertainties and unknown factors related to this reaction will be discussed further in Sect. 3.2.4.

When panels (a) and (c) in Fig. 5 are compared, it can be seen that the  $\Omega_{\text{CMAQ}}$  is in general greatly larger than the  $\Omega_{\text{OMI}}$  over the regions with strong NO<sub>x</sub> emissions. This was also presented in Han et al. (2011). The large differences between the two NO<sub>2</sub> columns can be confirmed again in panel (d) of Fig. 5. However, such a comparison without apply-

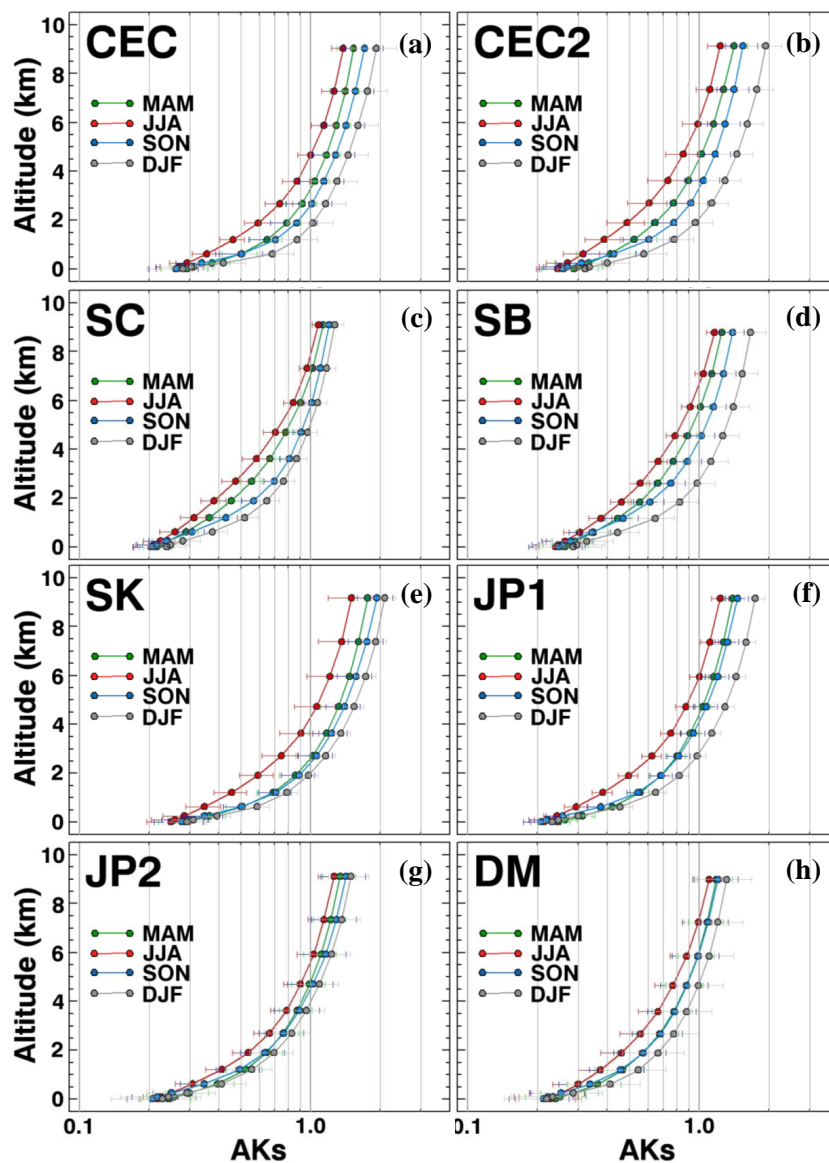


**Figure 3.** Vertical distributions of averaging kernels (AKs) with error bars (one-sigma standard deviations from the mean) for four seasons over (a) CEC, (b) CEC2, (c) SC, (d) SB, (e) SK, (f) JP1, (g) JP2, and (h) DM regions (refer to Fig. 2 regarding the regions of analysis).

ing the AKs is like comparing apples and oranges, and is not reasonable. Such studies have been conducted over East Asia with misleading conclusions (e.g., Ma et al., 2006; He et al., 2007; Uno et al., 2007; Shi et al., 2008; Han et al., 2009, 2011). In this context, we now wish to correct our previous conclusions (Han et al., 2011) here, applying the AKs to the CMAQ model simulations, using the linear relationship presented in Eq. (2).

After the application of the AKs to the CMAQ model simulations, the comparison becomes independent of the a priori profile shape used in the NO<sub>2</sub> retrieval process (Esques and Boersma, 2003). In this study, when the panels (b) and (c) in Fig. 5 are compared, it can be seen that the CMAQ-calculated NO<sub>2</sub> columns considering the AKs are much more compara-

ble to the OMI-retrieved NO<sub>2</sub> columns, possibly indicating that the bottom-up NO<sub>x</sub> emission used in the CMAQ model simulations would not be very greatly overestimated, unlike the previous conclusion drawn by Han et al. (2011). Figure 5d and e more directly show the effects of the application of the AKs. When the AKs are applied, the differences are greatly diminished, and are even negative, particularly over the CEC regions. The  $\Omega_{\text{CMAQ,AK}}$  becomes smaller than the  $\Omega_{\text{OMI}}$  over the CEC, SC, SK, JP1, and JP2 regions. Also, possible overestimations of the bottom-up NO<sub>x</sub> emissions were found in the CEC2 and SB regions, particularly during the winter. Possible underestimations over the CEC and SC regions and overestimations over the SB and CEC2 regions were also presented in the study of Lin (2012). In Lin (2012),

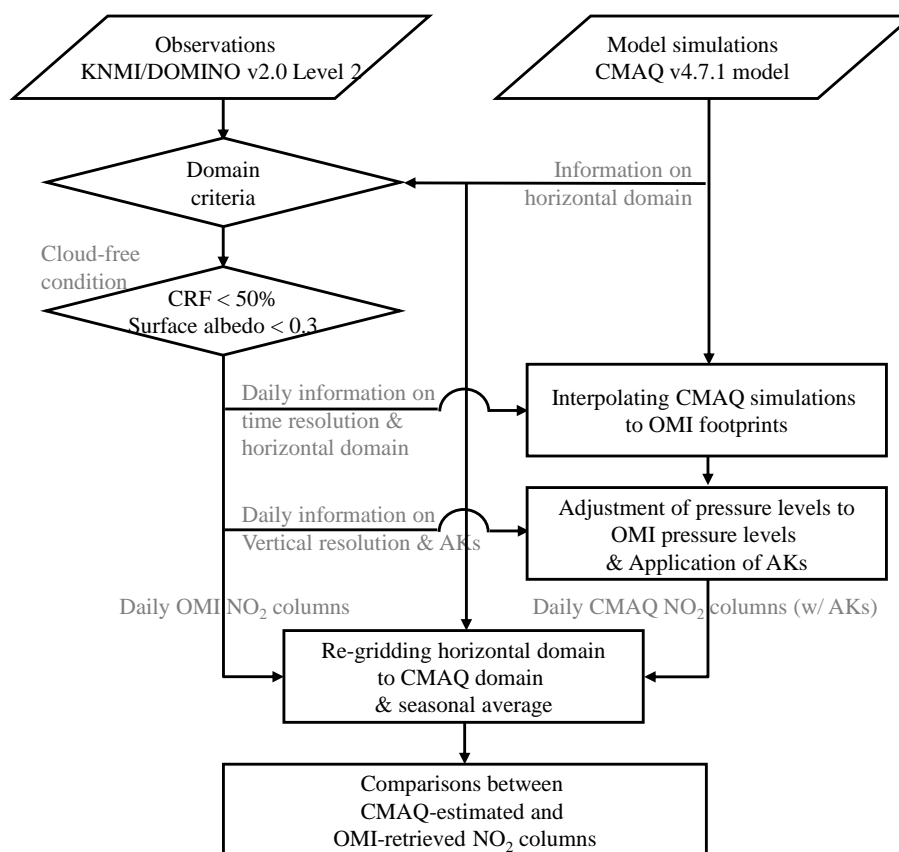


**Figure 4.** Flow diagram for direct comparison between CMAQ-estimated and OMI-retrieved NO<sub>2</sub> columns.

the  $\Omega_{\text{GOES-CHEM,AK}}$  values were found to be about 20 and 36 % lower than the  $\Omega_{\text{OMI}}$  over eastern China in summer and winter, respectively, whereas in the calculations herein, the respective  $\Omega_{\text{CMAQ,AK}}$  values were about 57 % and 5 % lower than the  $\Omega_{\text{OMI}}$  over eastern China. These differences would be caused by the constant NO<sub>x</sub> emission fluxes and relatively coarse horizontal resolutions ( $0.67^\circ \times 0.5^\circ$ ) used in the GEOS-CHEM simulations performed by Lin (2012).

In Table 2, we summarize the seasonal average tropospheric NO<sub>2</sub> columns and normalized mean errors (NMEs, defined in Table A1) with and without considering the AKs for the eight focus regions. It can be seen that the NMEs (with AKs applied) ranged from 40.3 to 63.2 % over the entire domain in Table 2. Although the differences between  $\Omega_{\text{CMAQ,AK}}$  and  $\Omega_{\text{OMI}}$  were the smallest during the summer (as shown in Fig. 5), the NMEs showed the largest values during summer. The reasons for this are discussed in detail in Sect. 3.1.2.

Collectively, the seasonal and regional (spatial) characteristics observed from the OMI sensor were found to be captured well by the CMAQ model simulations using the INTEX-B, CAPSS, and REAS emission inventories. However, some regional discrepancies between the two NO<sub>2</sub> columns were also found, particularly during winter, indi-

cating possible underestimation of the NO<sub>x</sub> emissions over the CEC and SC regions as well as overestimation over the CEC2 and SB regions in the CMAQ model simulations. To further investigate the eight regions of interest, scatter plots and statistical analyses were carried out in Sect. 3.1.2.

### 3.1.2 Scatter plots and statistical analyses

Figure 6 presents the seasonal scatter plot analysis between the  $\Omega_{\text{CMAQ,AK}}$  and  $\Omega_{\text{OMI}}$  for the eight focus regions defined in Fig. 2. The statistical analysis related to the scatter plots was also conducted in terms of the Pearson correlation coefficient ( $R$ ), linear regression slope ( $S$ ), and  $y$  intercept ( $Y-I$ ). As mentioned in Sect. 2.2, seasonal average of the daily  $\Omega$  was taken to reduce the random errors which have occurred during the NO<sub>2</sub> measurement and retrieval processes (Fioletov et al., 2002; Monaghan et al., 2006; Johnson et al., 2007; Richter et al., 2011; Clarisse et al., 2013). The use of seasonally averaged data improved the correlation coefficients from 0.49–0.63 to 0.78–0.88 over the entire domain (DM) (regarding this issue, readers can compare Fig. 6 with Fig. S1 in the Supplement). Although the correlation coefficients were sometimes lower than 0.7 in Fig. 6, the two NO<sub>2</sub> columns correlated well, with  $R$  values between 0.71 and 0.96 (also, refer to the “ $R$ ” values colored in Fig. 7). Slopes lower than

**Table 2.** Average tropospheric NO<sub>2</sub> columns, standard deviations, and the normalized mean error (NME) with and without the application of AKs for four seasons.

Region	Season	$n^a$	$\Omega_{\text{CMAQ}}$ (w/o AKs) <sup>b</sup>	$\Omega_{\text{CMAQ,AK}}$ (w/ AKs) <sup>b</sup>	$\Omega_{\text{OMI}}^b$	NME (w/o AKs)	NME (w/ AKs)
CEC	Spring	900	11.68 (6.19) <sup>c</sup>	6.40 (3.95) <sup>c</sup>	6.89 (4.07)	74.48	29.48
	Summer	900	6.43 (4.09)	2.60 (1.80)	5.29 (3.02)	45.55	53.06
	Fall	900	13.29 (7.71)	7.18 (5.04)	9.49 (5.89)	52.08	32.79
	Winter	900	16.95 (9.52)	11.08 (7.52)	14.18 (8.05)	37.52	31.77
CEC2	Spring	820	10.49 (6.34)	4.79 (4.12)	4.45 (3.98)	135.72	29.75
	Summer	820	6.01 (6.16)	2.31 (2.92)	3.02 (2.15)	102.70	39.44
	Fall	820	12.36 (7.44)	5.84 (4.39)	4.97 (3.97)	148.85	36.61
	Winter	820	20.07 (6.84)	11.24 (5.54)	8.49 (5.79)	136.26	42.58
SC	Spring	1125	3.79 (2.87)	1.16 (1.04)	2.20 (2.03)	81.80	50.26
	Summer	1124	2.65 (2.57)	0.76 (0.85)	1.77 (1.73)	65.26	57.83
	Fall	1125	3.79 (2.79)	1.27 (1.02)	2.20 (2.31)	79.89	44.80
	Winter	1125	8.98 (4.06)	3.21 (1.88)	3.24 (3.39)	181.26	36.41
SB	Spring	408	4.25 (2.84)	1.53 (1.09)	2.56 (1.55)	80.16	44.97
	Summer	420	2.34 (1.66)	0.78 (0.59)	2.14 (0.99)	39.86	63.31
	Fall	418	6.37 (4.47)	2.34 (1.76)	2.71 (2.15)	143.93	43.75
	Winter	403	11.55 (7.69)	5.31 (4.14)	3.43 (3.01)	237.75	72.46
SK	Spring	260	9.14 (5.78)	4.95 (3.50)	5.24 (3.74)	75.37	26.93
	Summer	260	7.52 (7.94)	3.06 (3.60)	3.41 (2.58)	128.05	42.73
	Fall	260	8.85 (6.60)	4.60 (3.71)	4.81 (3.62)	93.57	38.81
	Winter	260	12.30 (5.69)	6.82 (3.37)	6.68 (4.14)	88.42	29.78
JP1	Spring	204	4.61 (1.51)	2.03 (0.73)	3.58 (2.48)	44.83	45.50
	Summer	204	2.47 (1.06)	0.77 (0.33)	2.91 (1.98)	34.88	73.42
	Fall	204	4.62 (1.92)	1.91 (0.90)	3.57 (2.50)	41.81	48.26
	Winter	204	7.63 (2.88)	3.47 (1.41)	4.48 (3.07)	74.66	36.95
JP2	Spring	285	3.90 (3.27)	1.72 (1.75)	3.09 (2.96)	36.19	45.69
	Summer	286	2.41 (2.08)	0.86 (0.81)	2.64 (2.77)	29.99	67.72
	Fall	286	3.96 (3.33)	1.63 (1.66)	3.12 (3.17)	31.95	47.71
	Winter	279	5.84 (4.60)	2.56 (2.45)	3.92 (4.20)	55.64	42.72
Entire domain	Spring	15175	3.02 (4.46)	1.35 (2.39)	1.97 (2.43)	80.49	45.85
	Summer	15207	1.76 (3.09)	0.64 (1.29)	1.59 (1.72)	59.27	63.15
	Fall	15224	3.31 (5.13)	1.45 (2.72)	2.06 (3.05)	78.78	44.27
	Winter	14075	5.97 (7.31)	2.96 (4.52)	3.20 (4.79)	98.13	40.31

<sup>a</sup> The number of data; <sup>b</sup> Unit,  $\times 10^{15}$  molecules  $\text{cm}^{-2}$ ; <sup>c</sup> Standard deviations of the distributions of tropospheric NO<sub>2</sub> columns.

1.0 (see dashed lines in Fig. 6) were found in the “blue” regions in Fig. 5e such as the CEC, SC, SB, JP1, and JP2 regions. These low slopes indicate the possible “underestimation” of the bottom-up NO<sub>x</sub> emissions used in the CMAQ model simulations, as discussed in Sect. 3.1.1.

Further statistical analyses were conducted. For absolute differences, mean error (ME) and mean bias (MB) were utilized. For relative differences, mean normalized gross error (MNGE), mean normalized bias (MNB), normalized mean error (NME), normalized mean bias (NMB), mean fractional error (MFE), and mean fractional bias (MFB) were used. The Pearson correlation coefficient ( $R$ ) and index of agreement (IOA) were also analyzed to assess the degrees of

correlations and agreement, respectively. These 10 performance metrics are defined and described in Table A1 (see Appendix A).

Figure 7 summarizes the seasonal statistical analyses for eight focus regions. Light colors were used to indicate good agreements, while dark colors marked poor agreements. As shown, the IOAs (as a measure of the degree of model prediction errors, Willmott, 1981) showed high values, between 0.78 and 0.93, over the entire domain. However, the IOAs sometimes showed relatively low values during the summer over several regions where large relative differences were found (e.g., SB, JP1, and JP2 regions during the summer), because the IOA decreased with the large differ-



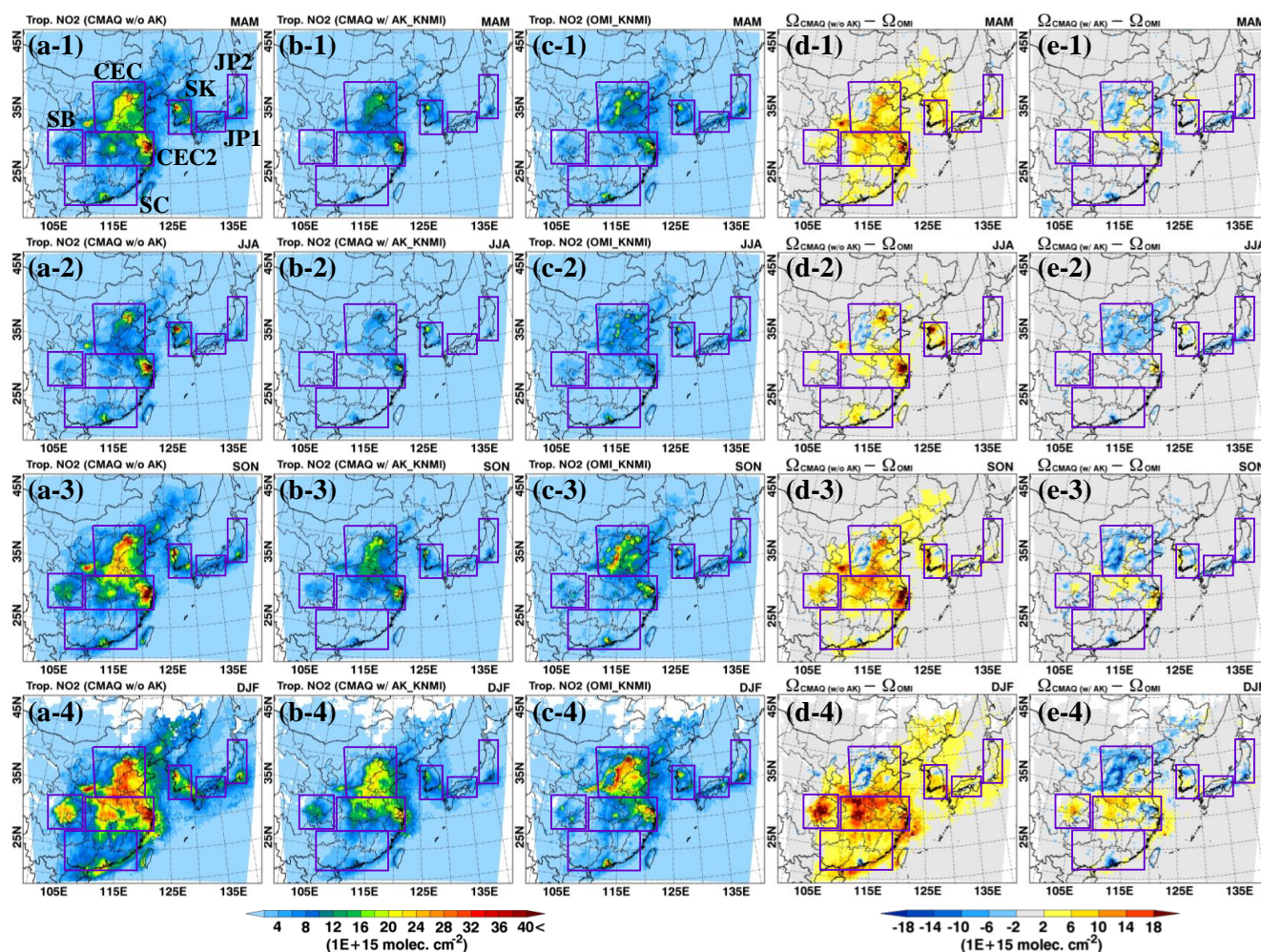


**Figure 5.** Spatial and seasonal distributions of CMAQ-calculated tropospheric NO<sub>2</sub> columns (a) without the applications of the AKs and (b) with the AKs and (c) OMI-retrieved NO<sub>2</sub> columns from the KNMI algorithm. Differences between OMI-retrieved and CMAQ-calculated NO<sub>2</sub> columns (d) before the applications of the AKs and (e) after the applications of the AKs.

ence between  $\Omega_{\text{CMAQ,AK}}$  and  $\Omega_{\text{OMI}}$ . As shown in Fig. 7, large MEs were found over the CEC region ( $2.03 \times 10^{15}$  to  $4.51 \times 10^{15}$  molecules  $\text{cm}^{-2}$ ) and MBs mostly ranges between  $-1.78 \times 10^{15}$  and  $1.88 \times 10^{15}$  molecules  $\text{cm}^{-2}$  in East Asia, except in CEC. Again, the negative values of the MBs in Fig. 7 indicate that the NO<sub>x</sub> emissions used were possibly underestimated.

In the seasonal perspective, all statistical parameters of the relative differences (i.e., MNGE, MNB, NME, NMB, MFE, and MFB) showed large values for the summer in all the regions, because the OMI-retrieved quantity in the denominator of the equations (see Table A1) for the summer were relatively small versus the values of the absolute differences in the numerator. In this study, the  $\Omega_{\text{CMAQ,AK}}$  values over the entire domain were 7.3 and 59.7 % smaller than  $\Omega_{\text{OMI}}$  in terms of the NMB during the summer and winter seasons, respectively. In the regional perspective, the relative differences showed large values in the SC, SB, JP1, and JP2 re-

gions, where the  $\Omega$  were relatively low (i.e., the same reason leading to larger relative errors and biases in the summer). In this study, the  $\Omega_{\text{CMAQ,AK}}$  values during winter were found to be 21.8 % smaller than the  $\Omega_{\text{OMI}}$  over CEC, but 32.3 % and 54.7 % larger over CEC2 and SB, respectively. Collectively, the statistical analyses showed that the  $\Omega_{\text{CMAQ,AK}}$  were, on annual average,  $\sim 28$  % (from 7 % to 60 % with seasonal variation) smaller than the  $\Omega_{\text{OMI}}$ , indicating that the NO<sub>x</sub> emissions for East Asia were possibly underestimated.

### 3.2 Sensitivity analyses

After the application of the AKs, both the  $\Omega_{\text{CMAQ,AK}}$  and  $\Omega_{\text{OMI}}$  became much more comparable with each other as shown in Fig. 5. Even so, this comparison study still has several uncertainties. Because of the uncertainties, it is difficult to directly relate the differences between the  $\Omega_{\text{CMAQ,AK}}$  and  $\Omega_{\text{OMI}}$  to under- or over-estimations in the NO<sub>x</sub> emissions.

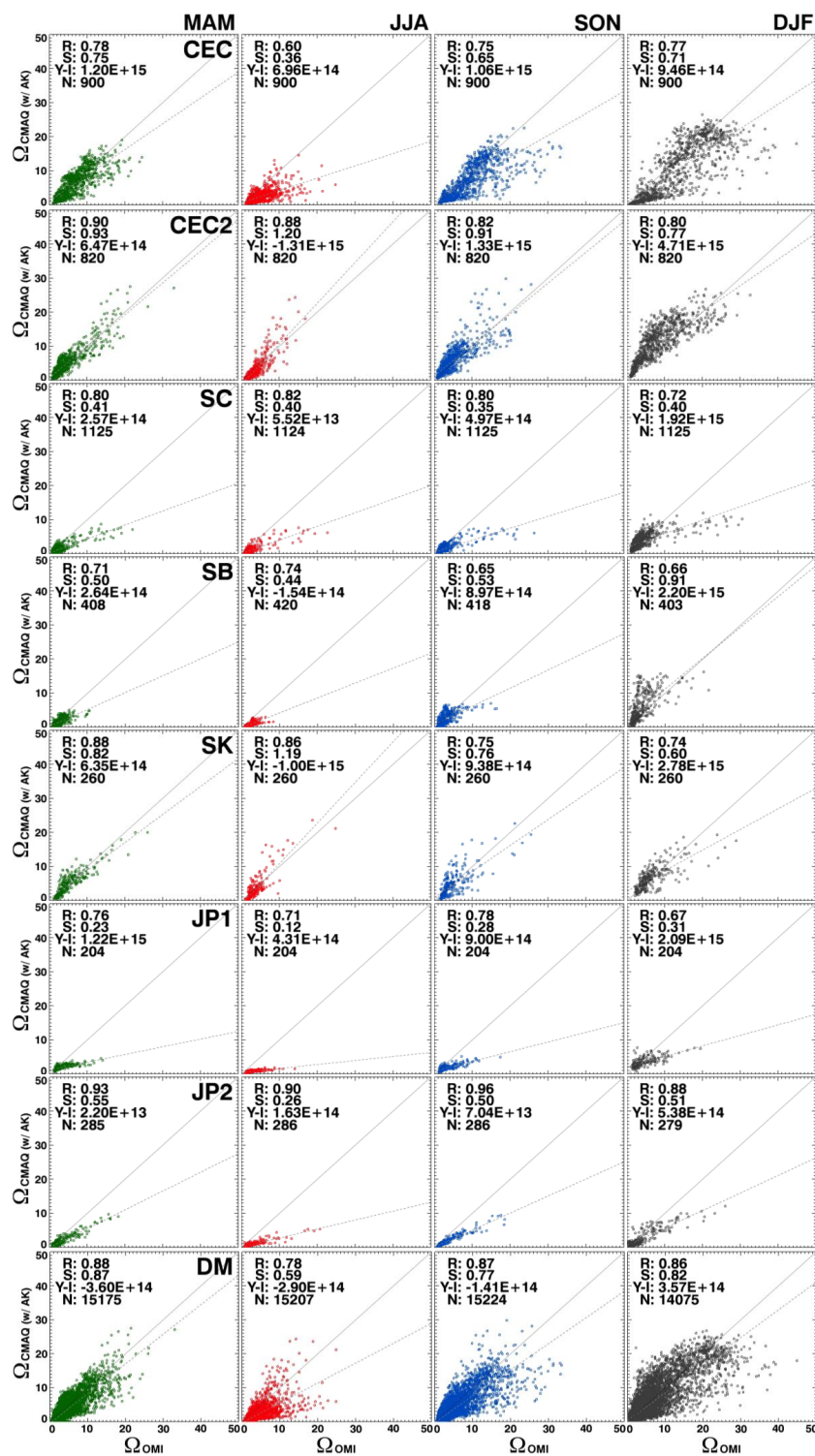


**Figure 6.** Seasonal scatter plots between CMAQ-calculated and OMI-retrieved NO<sub>2</sub> columns (Unit:  $\times 10^{15}$  molecules  $\text{cm}^{-2}$ ) using seasonally averaged data sets over the CEC, CEC2, SC, SB, SK, JP1, JP2, and DM regions. Here, the AKs were applied to the CMAQ model simulations. *R*, *S*, *Y-I*, and *N* represent the correlation coefficient, linear regression slope, y intercept, and the number of data points, respectively.

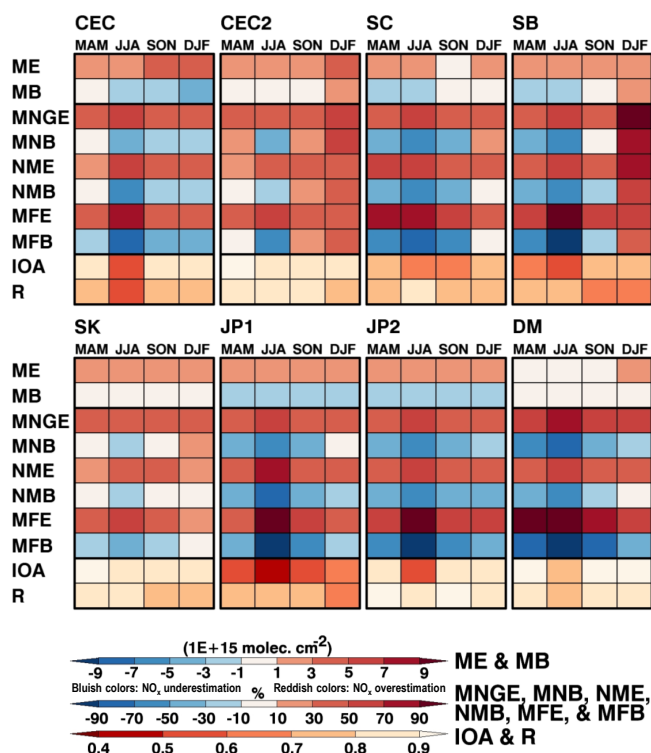


**Figure 7.** Statistical analyses between CMAQ-calculated and OMI-retrieved NO<sub>2</sub> columns using the performance metrics defined in Table A1. Here, the color bars represent ME and MB at the top, MNGE, MNB, NME, NMB, MFE, and MFB in the middle, and IOA and *R* at the bottom. Here, light colors show good agreements, while dark colors indicate poor agreements.

Therefore, examination of the uncertainty issues was carried out herein. The issues selected for examination in this study were as follows: (i) the monthly variation in NO<sub>x</sub> emissions; (ii) influences of the different magnitude of NO<sub>x</sub> emissions; and (iii) different parameterizations of the reaction probability of N<sub>2</sub>O<sub>5</sub> onto aerosols in the CMAQ model simulations. These three issues were selected for the following reasons: (i) the emission flux in East Asia is believed to be one of the most uncertain factors, and its magnitude can vary greatly depending on monthly variation as well as methodology and activity data used to estimate the emission fluxes (Cases 2 and 3) (Wang et al., 2007; Zhang et al., 2007, 2009; Han et al., 2009; Klimont et al., 2009; Xing et al., 2011); and (ii) although the condensation of N<sub>2</sub>O<sub>5</sub> radicals is a major NO<sub>x</sub> loss processes during the winter and thus may significantly influence the tropospheric NO<sub>2</sub> columns, the magnitudes of  $\gamma_{\text{N}_2\text{O}_5}$  remain highly uncertain, ranging between 0.1 and 0.001 (Case 4) (Dentener and Crutzen, 1993; Jacob, 2000; Brown et al., 2006; Davis et al., 2008; Macintyre and Evans, 2010). Sect. 3.2 is therefore devoted to these issues, which are addressed with sensitivity analyses.

### 3.2.1 Monthly variation in NO<sub>x</sub> emissions: Case 2

First, the monthly variations of NO<sub>x</sub> emissions over China were investigated, choosing different monthly variations from the base-case emission. In this sensitivity run (see Table 1), we applied a more drastic/extreme monthly variation of the NO<sub>x</sub> emissions (thick black line in Fig. 1) (Han et al., 2009) to the CMAQ model simulation over China in this 1-year run. The main reason we did this is that, as shown in Figs. 5 and 6, the  $\Omega_{\text{CMAQ,AK}}$  was smaller than the  $\Omega_{\text{OMI}}$ , over several main regions (such as CEC and main megacity areas like Hong Kong and Shanghai) in China, particularly during the “cold months”. It should be noted that during the cold months, the NO<sub>x</sub> emission fluxes reported in Han et al. (2009) for China were 1.20 times larger than those from the INTEX-B inventory.

The results are presented in Fig. 8. The spatial distributions of the  $\Omega_{\text{CMAQ,AK}}$  and  $\Omega_{\text{OMI}}$  are shown in Fig. 8 for the four seasons. As indicated in Table S1 in the Supplement, the application of the AKs again greatly reduced the errors and biases between the two tropospheric NO<sub>2</sub> columns in this sensitivity test. As expected, the  $\Omega_{\text{CMAQ,AK}}$  in Fig. 8a generally increased for the spring and winter, whereas it decreased for the summer and fall, compared with the values in Fig. 5b. These increases in the  $\Omega_{\text{CMAQ,AK}}$  for the winter produced better agreement with the  $\Omega_{\text{OMI}}$ , particularly over the CEC region, showing that the MBs over CEC during the winter decreased from  $-3.10 \times 10^{15}$  to  $-7.42 \times 10^{14}$  molecule cm<sup>-2</sup> (see the average NO<sub>2</sub> columns and NMEs in Tables 2 and S1). However, as shown in Tables 2 and S1, the situations became worse, except for the CEC region, showing significant increases in NMEs, compared with the NMEs in cases using the monthly variation of the INTEX-B inventory taken from Zhang et al. (2009). Even larger (more serious) differences between the two NO<sub>2</sub> columns in Fig. 8c were found over other regions of China (CEC2, SC, and SB) than those shown in Fig. 5e in terms of errors and biases. For example, the MBs during the winter increased from  $2.74 \times 10^{15}$ ,  $-2.92 \times 10^{13}$ , and  $1.88 \times 10^{15}$  molecule cm<sup>-2</sup> to  $5.26 \times 10^{15}$ ,  $7.10 \times 10^{15}$ , and  $5.35 \times 10^{15}$  molecule cm<sup>-2</sup> over CEC2, SC, and SB, respectively.

Further detailed analyses over the eight focus regions were carried out, and the scatter plots and statistical analyses are presented in Figs. S2 and S3. Collectively, the sensitivity test showed that the monthly variations of the OMI observations were better captured by the CMAQ model simulations using the monthly variations of the INTEX-B inventory than those from Han et al. (2009), although the monthly variations in the NO<sub>x</sub> emission of the INTEX-B inventory still remain uncertain in China, particularly over the CEC region.

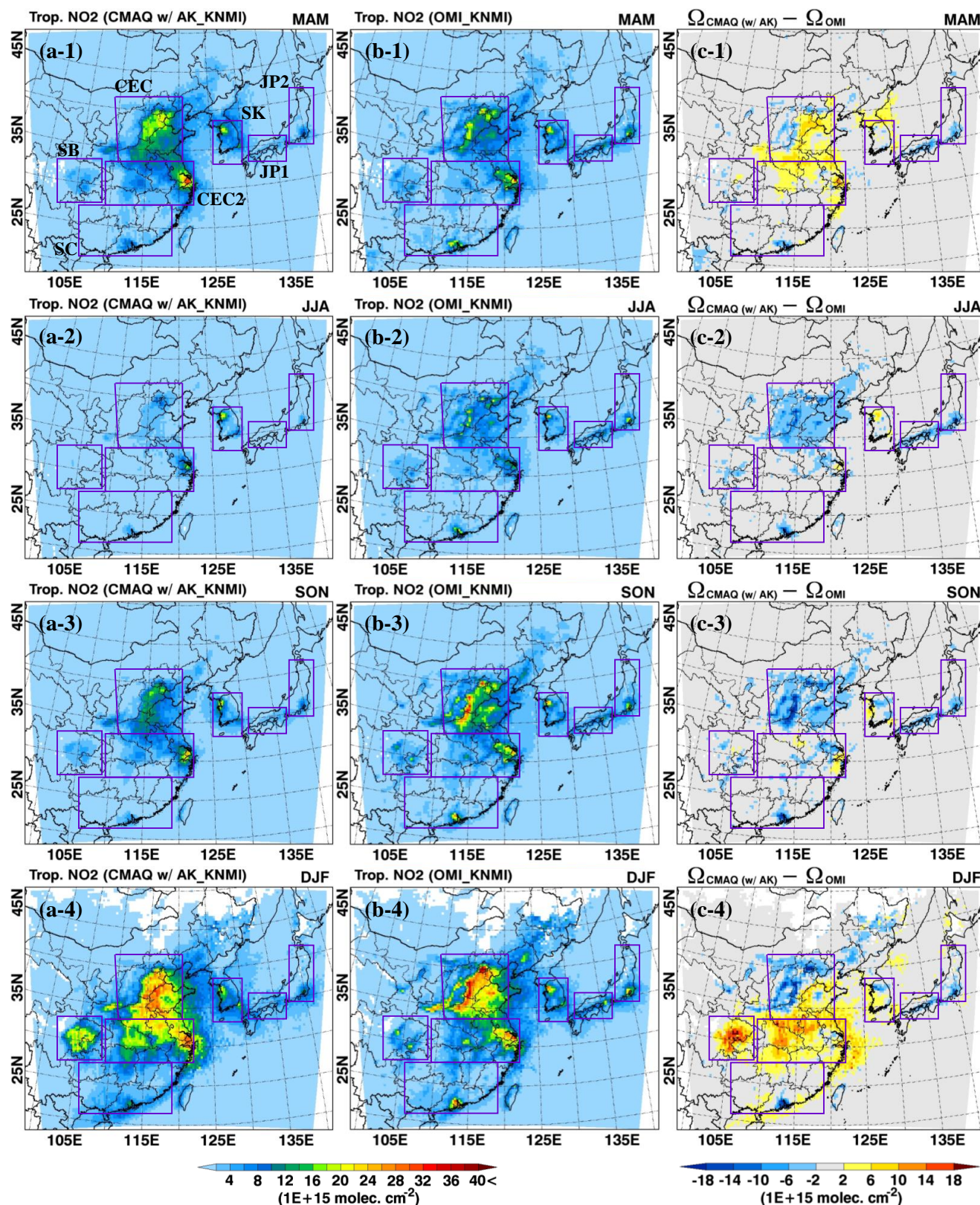


**Figure 8.** Spatial distributions of (a) CMAQ-calculated NO<sub>2</sub> columns with the AKs and (b) OMI-retrieved NO<sub>2</sub> columns and (c) their differences for four seasonal episodes. Here, the monthly variations of NO<sub>x</sub> emissions from Han et al. (2009) were applied to the CMAQ model simulations.

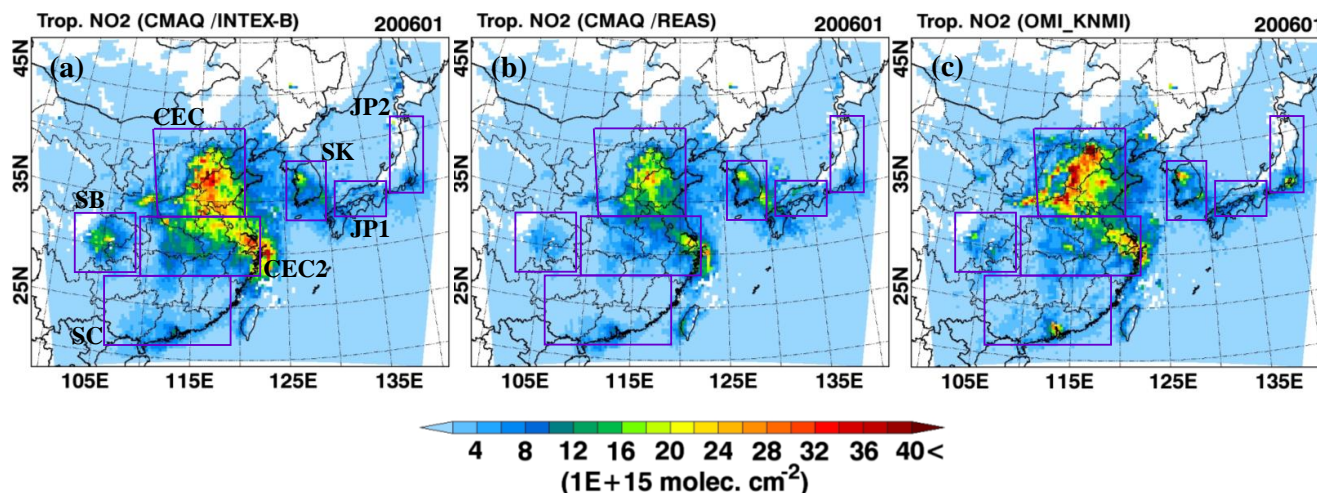


**Figure 9.** CMAQ-calculated NO<sub>2</sub> columns using (a) INTEX-B inventory and (b) REAS inventory over China and (c) OMI-observed NO<sub>2</sub> columns for January.

### 3.2.2 Another NO<sub>x</sub> emission inventory (REAS v1.11): Case 3

There is another NO<sub>x</sub> emission inventory available in China: the REAS v1.11 emission inventory for 2006 (Ohara et al., 2007). Thus, in this section, the REAS emission inventory, a frequently used bottom-up inventory established by the National Institute of Environmental Studies (NIES) in Japan, was tested over China for January (a cold month) in order to determine the influence of different NO<sub>x</sub> emissions on the tropospheric NO<sub>2</sub> columns. Because the REAS v1.11 inventory does not include monthly variation, the same monthly variation of the INTEX-B inventory was also applied to this sensitivity study. The NO<sub>x</sub> emissions between the INTEX-B and REAS inventories differed greatly over China. For example, the annual NO<sub>x</sub> emissions from the INTEX-B inventory were 2.48, 2.22, 1.60, and 0.57 Tg N yr<sup>-1</sup> over the CEC, CEC2, SC, and SB regions, respectively, whereas those from the REAS inventory were 1.93, 1.56, 1.40, and 0.40 Tg N yr<sup>-1</sup>, respectively, over the same regions.

The results are presented in Fig. 9 and Table S2. The application of the AKs to the CMAQ model simulations were also taken into account in this comparison (see Table S2). As expected, the  $\Omega_{\text{CMAQ,AK}}$  decreased significantly over China, when the REAS NO<sub>x</sub> emissions were used (refer to Table S2). Although the absolute differences between the  $\Omega_{\text{CMAQ,AK}}$  and  $\Omega_{\text{OMI}}$  became smaller over the CEC2 and SB regions, much large underestimates were found over the CEC region, compared with the case of the INTEX-B inventory as shown in Fig. 9.

Collectively, our results indicate that (i) the NO<sub>x</sub> emission fluxes from the REAS inventory are also underestimated over China (particularly, over the CEC region), (ii) both NO<sub>x</sub> emission inventories (INTEX-B and REAS) showed under-

estimation over the CEC region and the Hong Kong area, and (iii) accurate spatial distributions of NO<sub>x</sub> emissions and the magnitude of NO<sub>x</sub> emissions were important factors to reduce the degree of disagreement between the CTM-estimated and satellite-retrieved NO<sub>2</sub> columns. For better agreement between the  $\Omega_{\text{CMAQ,AK}}$  and  $\Omega_{\text{OMI}}$  over China, a combination of the two emission inventories may be a good practical attempt in the CMAQ model simulations over East Asia, based on this result. That is, the INTEX-B NO<sub>x</sub> emissions data tended to produce better results over the CEC region, whereas the REAS NO<sub>x</sub> emissions data tended to generate better results over the CEC2 and SB regions. However, this issue (i.e., the combination of the two emission inventories) needs to be examined using a more sophisticated approach, and should be investigated further.

### 3.2.3 Reaction probability of N<sub>2</sub>O<sub>5</sub>: Case 4

We explored the issue of reaction probability of N<sub>2</sub>O<sub>5</sub> ( $\gamma_{\text{N}_2\text{O}_5}$ ) onto aerosols, because a relatively large discrepancy between the  $\Omega_{\text{CMAQ,AK}}$  and  $\Omega_{\text{OMI}}$  was found, particularly during the winter season. During the winter season, the condensation of N<sub>2</sub>O<sub>5</sub> into atmospheric particles is an important NO<sub>x</sub> loss process (Dentener and Crutzen, 1993; Brown et al., 2004, 2006). Thus, it can affect the CMAQ-simulated NO<sub>2</sub> columns ( $\Omega_{\text{CMAQ,AK}}$ ). Although it is an important physicochemical NO<sub>x</sub> loss process during the winter, the magnitude of  $\gamma_{\text{N}_2\text{O}_5}$  has been a controversial issue. In this study, five  $\Omega_{\text{CMAQ,AK}}$  from the CMAQ model simulations with five different  $\gamma_{\text{N}_2\text{O}_5}$  parameterizations were compared with the  $\Omega_{\text{OMI}}$  over East Asia. These five parameterizations are from the works of (i) Dentener and Crutzen (1993), (ii) Riemer et al. (2003), (iii) a combination of Riemer et al. (2003) and Evans and Jacob (2005), (iv) Davis et al. (2008), and (v) Brown et al. (2006). The mathematical expressions for these

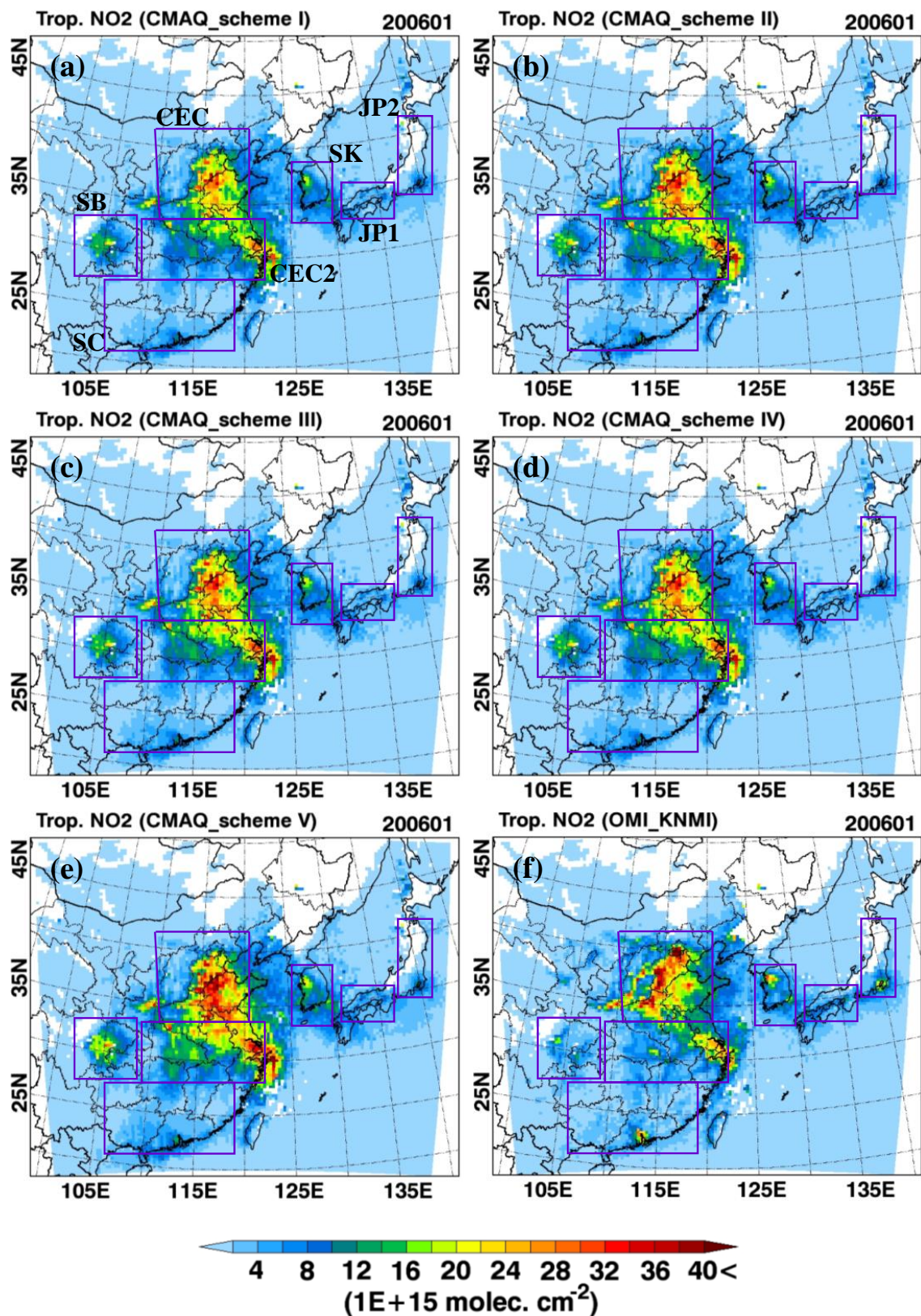


**Figure 10.** CMAQ-calculated NO<sub>2</sub> columns using five  $\gamma_{\text{N}_2\text{O}_5}$  parameterizations from (a) Dentener and Crutzen (1993), (b) Riemer et al. (2003), (c) combination of Riemer et al. (2003) and Evans and Jacob (2005), (d) Davis et al. (2008), and (e) Brown et al. (2006) and (f) OMI-observed NO<sub>2</sub> columns for January.

**Table 3.** Reaction probabilities of N<sub>2</sub>O<sub>5</sub> onto aerosol surfaces.

References	Condensing medium	Reaction probability of N <sub>2</sub> O <sub>5</sub> ( $\gamma_{\text{N}_2\text{O}_5}$ )
Dentener and Crutzen (1993) <sup>a</sup> (Scheme I Fig. 10a)	Aqueous particles	$\gamma_{\text{N}_2\text{O}_5} = 0.1$
Jacob (2000) <sup>a,b</sup>	Aqueous particles	$\gamma_{\text{N}_2\text{O}_5} = 0.1$ (Range: 0.01–1)
Tie et al. (2003) <sup>a</sup>	Aqueous particles	$\gamma_{\text{N}_2\text{O}_5} = 0.04$ (Range: 0.0–0.10)
Rierner et al. (2003) <sup>a</sup> (Scheme II in Fig. 10b)	Sulfate and Nitrate	$\gamma_{\text{N}_2\text{O}_5} = f \times \gamma_1 + (1 - f) \times \gamma_2$ (Range: 0.02–0.002)  $\gamma_1 = 0.02, \gamma_2 = 0.002; f = \frac{m_{\text{SO}_4^{2-}}}{m_{\text{SO}_4^{2-}} + m_{\text{NO}_3^-}}$ $m_{\text{SO}_4^{2-}}$ and $m_{\text{NO}_3^-}$ : aerosol mass concentrations of sulfate and nitrate, respectively
Evans and Jacob (2005) <sup>a</sup>	Sulfate  OC  BC Sea salt  Dust	$\gamma_{\text{N}_2\text{O}_5} = \alpha \times 10^\beta$ $\alpha = 2.79 \times 10^{-4} + 1.3 \times 10^{-4} \times \text{RH} - 3.43 \times 10^{-6} \times \text{RH}^2 + 7.52 \times 10^{-8} \times \text{RH}^3$ $\beta = 4 \times 10^{-2} \times (294 - T) (T \geq 282 \text{ K})$ $\beta = 0.48 (T < 282 \text{ K})$ $\gamma_{\text{N}_2\text{O}_5} = \text{RH} \times 5.2 \times 10^{-4} (\text{RH} < 57 \%)$ $\gamma_{\text{N}_2\text{O}_5} = 0.03 (\text{RH} \geq 57 \%)$ $\gamma_{\text{N}_2\text{O}_5} = 0.005$ $\gamma_{\text{N}_2\text{O}_5} = 0.005 (\text{RH} < 62 \%)$ $\gamma_{\text{N}_2\text{O}_5} = 0.03 (\text{RH} \geq 62 \%)$ $\gamma_{\text{N}_2\text{O}_5} = 0.01$ RH: relative humidity (%); T: temperature (K)
Combination of parameterization by Evan and Jacob (2005) and Rierner et al. (2003) <sup>a</sup> (Scheme III in Fig. 10c)	Sulfate and Nitrate	$\gamma_{\text{N}_2\text{O}_5} = f \cdot \gamma_1 + (1 - f) \cdot \gamma_2$  $\alpha = 2.79 \times 10^{-4} + 1.3 \times 10^{-4} \times \text{RH} - 3.43 \times 10^{-6} \times \text{RH}^2 + 7.52 \times 10^{-8} \times \text{RH}^3$ $f = \frac{m_{\text{SO}_4^{2-}}}{m_{\text{SO}_4^{2-}} + m_{\text{NO}_3^-}}$ $\gamma_1 = \alpha \times 10^{0.48}; \gamma_2 = 0.1 \times \gamma_1 (T < 282 \text{ K})$ $\gamma_1 = \alpha \times 10^\beta; \gamma_2 = 0.1 \times \gamma_1; \beta = 4 \times 10^{-2} \times (294 - T) (T \geq 282 \text{ K})$
Davis et al. (2008) <sup>a</sup> (Scheme IV in Fig. 10d)	Aqueous particles  Bisulfate ( $i = 1$ ) Sulfate ( $i = 2$ ) Nitrate ( $i = 3$ )  Dry particles	$\gamma_{\text{N}_2\text{O}_5, \text{mix}} = \sum_{i=1}^3 x_i \cdot \gamma_i$ $x_1 = 1 - (x_2 + x_3)$ for bisulfate $x_2 = \max\left(0, \min\left(1 - x_3, \frac{c_{\text{Ammo}}}{c_{\text{Nit}} + c_{\text{Sulf}}} - 1\right)\right)$ for sulfate $x_3 = \frac{c_{\text{Nit}}}{c_{\text{Nit}} + c_{\text{Sulf}}}$ for nitrate $\lambda_1 = -4.559088 + 2.8593 \times \text{RH} - 0.111201 \times T_{287}; \gamma_1 = \min\left(\frac{1}{1 + e^{-\lambda_1}}, 0.08585\right)$ $\lambda_2 = \lambda_1 - 0.369769; \gamma_2 = \min\left(\frac{1}{1 + e^{-\lambda_2}}, 0.053\right)$ $\lambda_3 = -0.8107744 + 4.9017 \times \text{RH}; \gamma_3 = \min\left(\frac{1}{1 + e^{-\lambda_3}}, 0.0154\right)$ $c_{\text{Ammo}}, c_{\text{Nit}},$ and $c_{\text{Sulf}}$ : molar concentration of ammonium, nitrate, and sulfate, respectively $\gamma_{\text{N}_2\text{O}_5, \text{mix}} = (x_1 + x_2) \gamma_d + x_3 \times \min(\gamma_d, \gamma_3)$ $\lambda_d = -6.133764 + 3.5920 \times \text{RH} - 0.196879 \times T_{293}; \gamma_d = \min\left(\frac{1}{1 + e^{-\lambda_d}}, 0.0124\right)$
Brown et al. (2006) <sup>b</sup> (Scheme V in Fig. 10e)		$\gamma_{\text{N}_2\text{O}_5} = \frac{4k_{\text{N}_2\text{O}_5}}{c_{\text{mean}} A}$  (i) $0.017 \pm 0.004$ (over Ohio and western Pennsylvania, US) (ii) $< 0.0010$ (over eastern Pennsylvania and New Jersey, US) (iii) $< 0.0016$ (over New York, US) $k_{\text{N}_2\text{O}_5}$ : rate constant ( $\text{s}^{-1}$ ); $c_{\text{mean}}$ : mean molecular speed of N <sub>2</sub> O <sub>5</sub> ( $\text{cm s}^{-1}$ ); A: aerosol surface density ( $\mu\text{m}^2 \text{cm}^{-3}$ )

<sup>a</sup> Modeling study; <sup>b</sup> Measurement study.

parameterizations are summarized briefly in Table 3. In the Dentener and Crutzen's parameterization (1993), they used a fixed value of  $\gamma_{\text{N}_2\text{O}_5}$  of 0.1 in their global CTM simulation (Scheme I in Table 3). In Rierner et al.'s parameteriza-

tion (2003),  $\gamma_{\text{N}_2\text{O}_5}$  is a main function of the acidity of the particles (Scheme II). In the combined parameterization of Evans and Jacob (2006) and Rierner et al. (2003),  $\gamma_{\text{N}_2\text{O}_5}$  is a function of relative humidity (RH), temperature, and the

acidity of the particles (Scheme III, standard scheme). In Davis et al.'s (2008) parameterization,  $\gamma_{\text{N}_2\text{O}_5}$  is a function of all the factors, such as RH, temperature, the acidity of the particles, and the mixing state (Scheme IV). Finally, for Brown et al.'s (2006) parameterization, we used a fixed minimum value of  $\gamma_{\text{N}_2\text{O}_5}$  of  $10^{-3}$  in the CMAQ model simulation (Scheme V).

The comparison results are presented in Fig. 10. As shown in Fig. 10 and Table 4, the  $\Omega_{\text{CMAQ,AK}}$  with the Brown et al. (2006) parameterization were  $\sim 19\%$  larger than those with the standard Scheme (III) over East Asia. This indicates that Brown et al.'s parameterization resulted in the smallest NO<sub>x</sub> loss rates (or nitrate formation rates) via this physicochemical reaction pathway.

In contrast, the application of the Dentener and Crutzen's parameterization to the CMAQ model simulation produced the smallest  $\Omega_{\text{CMAQ,AK}}$  in East Asia, indicating the fastest NO<sub>x</sub> loss rates, due to the large  $\gamma_{\text{N}_2\text{O}_5}$ . These results suggest that Brown et al.'s  $\gamma_{\text{N}_2\text{O}_5}$  ( $= 0.001$ ) may be smaller than the real value, while Dentener and Crutzen's  $\gamma_{\text{N}_2\text{O}_5}$  ( $= 0.1$ ) is probably larger. Other than Brown et al.'s and Dentener and Crutzen's parameterizations, it was found that there was almost no significant or practical difference in the  $\Omega_{\text{CMAQ,AK}}$  among the other three Schemes, II, III, and IV (also, refer to Table 4).

As shown in Fig. 10 and Table 4, Schemes II, III, and IV tended to produce better  $\Omega_{\text{CMAQ,AK}}$  data over East Asia than Schemes I and V, compared with  $\Omega_{\text{OMI}}$ . More recently, Brown et al. (2009) and Bertram et al. (2009) also discussed that the  $\gamma_{\text{N}_2\text{O}_5}$  values being used currently in regional/global CTMs were generally larger than those from their observed  $\gamma_{\text{N}_2\text{O}_5}$ . In addition to the issue of  $\gamma_{\text{N}_2\text{O}_5}$ , it should be noted that the aerosol surface density ( $A$ ) is another uncertain factor that can influence the  $\Omega_{\text{CMAQ,AK}}$ , because the rate constant ( $k_{\text{N}_2\text{O}_5}$ ) of the physicochemical reaction also depends on the aerosol surface density (refer to the Schwartz formula,  $k_{\text{N}_2\text{O}_5} = \frac{A \cdot c_{\text{mean}} \gamma_{\text{N}_2\text{O}_5}}{4}$ ). Although all of these issues are arguable, our results show that the  $\gamma_{\text{N}_2\text{O}_5}$  parameterizations can certainly influence the levels of  $\Omega_{\text{NO}_2}$  in East Asia, particularly during the winter season.

### 3.2.4 More uncertainties and outlooks

As mentioned previously, in this type of analysis all types of temporal variation are potentially important and should therefore be taken into account. A sensitivity analysis on the monthly variation in the NO<sub>x</sub> emissions in China was performed in Sect. 3.2.1, showing that the monthly variations in NO<sub>x</sub> emissions were an important factor. In contrast, there is only limited information on other temporal variation, such as daily and weekly variation in NO<sub>x</sub> emissions in East Asia. Unfortunately, no emission inventory in East Asia can provide us with this level of information. Regarding the issue of the temporal variation, the future Korean Geostationary Environmental Monitoring Spectrometer (GEMS) sen-

sor, which is planned to be launched in 2018, will be able to help to obtain such information on daily and weekly variation in the NO<sub>x</sub> emissions over East Asia (Kim, 2012).

There is also some level of uncertainty in the NO<sub>2</sub>-to-NO ratios, as discussed previously by Richter et al. (2005) and Han et al. (2009). This factor may be important, because every satellite remote-sensor monitors only NO<sub>2</sub> columns, not NO<sub>x</sub> columns. The NO<sub>2</sub>-to-NO ratios are affected seriously by anthropogenic and biogenic VOC (AVOC and BVOC) emissions and their mixing ratios. For example, if we assume a photostationary state, the NO<sub>2</sub>-to-NO ratios can be influenced by the mixing ratios of ozone and HO<sub>2</sub>, CH<sub>3</sub>O<sub>2</sub>, and RO<sub>2</sub> radicals, as shown in the following formula:

$$\frac{[\text{NO}_2]}{[\text{NO}]} = \frac{k_1[\text{O}_3] + k_2[\text{HO}_2] + k_3[\text{CH}_3\text{O}_2] + k_4[\text{RO}_2]}{J_1}, \quad (3)$$

where  $J_1$  is the NO<sub>2</sub> photolysis rate constant ( $\text{s}^{-1}$ ) and  $k_1$  ( $= 1.81 \times 10^{-14}$  at 298 K),  $k_2$  ( $= 8.41 \times 10^{-12}$  at 298 K),  $k_3$  ( $= 7.29 \times 10^{-12}$  at 298 K), and  $k_4$  ( $= 9.04 \times 10^{-12} - 2.80 \times 10^{-11}$  at 298 K) are the reaction rate constants ( $\text{cm}^3 \text{molecules}^{-1} \text{s}^{-1}$ ) for NO + O<sub>3</sub>, NO + HO<sub>2</sub>, NO + CH<sub>3</sub>O<sub>2</sub>, and NO + RO<sub>2</sub> reactions, respectively. Although  $k_1$  is the smallest among the 4 reaction rate constants, the NO<sub>2</sub> to-NO ratio tends to be determined by the NO + O<sub>3</sub> reaction, together with the photolysis of NO<sub>2</sub> ( $J_1$ ), because ambient O<sub>3</sub> mixing ratios usually occur in several tens of ppb. However, the NO + HO<sub>2</sub> and NO + RO<sub>2</sub> reactions during summer have almost equivalent (non-negligible) contribution to the NO<sub>2</sub>-to-NO ratios, for example, over the SC region where BVOC emissions are active. In addition, the mixing ratios of ozone, HO<sub>2</sub>, CH<sub>3</sub>O<sub>2</sub>, and RO<sub>2</sub> in Eq. (3) can be affected by AVOC and BVOC emissions and their mixing ratios, which are believed to be highly uncertain in East Asia (Fu et al., 2007; Lin et al., 2012; Han et al., 2013).

Third, as also discussed by Han et al. (2009), there is large uncertainty in the NO<sub>x</sub> loss rates (or NO<sub>x</sub> lifetime) in global/regional CTMs. Many groups have reported that the uncertainty in the NO<sub>x</sub> loss rate is related to several factors (Lin et al., 2012; Stavrou et al., 2013), such as nitric acid formation via the NO<sub>2</sub>+OH reaction (Atkinson et al., 2004; Mollner et al., 2010; Sander et al., 2011; Henderson et al., 2012) and NO + HO<sub>2</sub> reaction (Butkovskaya et al., 2005, 2009), isoprene chemistry (e.g., OH regeneration) during the summer months (Butler et al., 2008; Lelieveld et al., 2008; Archibald et al., 2010; Kubistin et al., 2010; Pugh et al., 2010), alkyl nitrate formation (Browne and Cohen, 2012; Browne et al., 2013), "daytime" HONO chemistry (Harris et al., 1982; Svennson et al., 1987; Rondon and Sanhueza, 1989; Pagsberg et al., 1997; Stemmler et al., 2006; Sörgel et al., 2011; Zhou et al., 2011), inclusion of in-plume photochemistry (Karamchandani et al., 2000; Song et al., 2003, 2010; Kim et al., 2009), and peroxyacetyl nitrate (PAN) formation (Roberts et al., 2002).

Recently, modeling uncertainties including meteorological parameters were discussed comprehensively by Lin



**Table 4.** Average tropospheric NO<sub>2</sub> columns, standard deviations and the ratios of the  $\Omega_{\text{CMAQ,AK}}$  to the  $\Omega_{\text{OMI}}$ , when different  $\gamma_{\text{N}_2\text{O}_5}$  parameterizations were applied to the CMAQ model simulations for January.

Region	Scheme <sup>a</sup>	$n^b$	$\Omega_{\text{CMAQ,AK}}^c$	$\Omega_{\text{OMI}}^c$	$R = \Omega_{\text{CMAQ,AK}}/\Omega_{\text{OMI}}$
CEC	Scheme I	896	11.11 (8.49) <sup>d</sup>	13.33 (9.00)	0.78
	Scheme II		12.40 (9.42)		0.87
	Scheme III		12.32 (9.35)		0.86
	Scheme IV		12.21 (9.27)		0.85
	Scheme V		14.23 (10.08)		0.99
CEC2	Scheme I	820	9.78 (6.14)	8.05 (6.34)	1.21
	Scheme II		11.37 (6.77)		1.41
	Scheme III		11.43 (6.82)		1.42
	Scheme IV		11.24 (6.74)		1.40
	Scheme V		13.53 (7.70)		1.68
SC	Scheme I	1125	2.47 (1.75)	2.98 (3.09)	0.83
	Scheme II		2.88 (1.88)		0.96
	Scheme III		2.80 (1.83)		0.94
	Scheme IV		2.77 (1.82)		0.93
	Scheme V		3.44 (2.06)		1.15
SB	Scheme I	386	5.05 (4.43)	3.34 (2.55)	1.51
	Scheme II		5.68 (4.83)		1.70
	Scheme III		5.43 (4.63)		1.63
	Scheme IV		5.44 (4.65)		1.63
	Scheme V		6.78 (5.65)		2.03
SK	Scheme I	260	6.80 (3.71)	6.70 (4.64)	1.01
	Scheme II		7.43 (3.83)		1.11
	Scheme III		7.29 (3.79)		1.09
	Scheme IV		7.26 (3.79)		1.08
	Scheme V		8.42 (4.03)		1.26
JP1	Scheme I	202	3.51 (1.75)	4.35 (2.58)	0.81
	Scheme II		3.96 (1.92)		0.91
	Scheme III		3.80 (1.86)		0.87
	Scheme IV		3.81 (1.87)		0.88
	Scheme V		4.34 (2.03)		1.00
JP2	Scheme I	192	2.69 (2.60)	4.68 (4.60)	0.57
	Scheme II		2.89 (2.73)		0.62
	Scheme III		2.81 (2.67)		0.60
	Scheme IV		2.82 (2.68)		0.60
	Scheme V		3.18 (2.84)		0.68
Entire domain	Scheme I	12901	2.88 (4.82)	3.23 (5.14)	0.89
	Scheme II		3.27 (5.40)		1.01
	Scheme III		3.22 (5.38)		1.00
	Scheme IV		3.20 (5.33)		0.99
	Scheme V		3.82 (6.22)		1.18

<sup>a</sup> Scheme I (Dentener and Crutzen, 1993), Scheme II (Riemer et al., 2003), Scheme III (combination of Riemer et al., 2003 and Evans and Jacob, 2005), Scheme IV (Davis et al., 2007), Scheme V (Brown et al., 2006); <sup>b</sup> The number of data; <sup>c</sup> Unit,  $\times 10^{15}$  molecules  $\text{cm}^{-2}$ ; <sup>d</sup> Standard deviations of the distributions of tropospheric NO<sub>2</sub> columns.

et al. (2012). They reported that when tropospheric NO<sub>2</sub> columns from several sensitivity simulations were compared with those from standard simulations, the largest impact on the tropospheric NO<sub>2</sub> columns was caused by modifying the reaction probability of HO<sub>2</sub> onto aerosols (i.e.,  $\gamma_{\text{HO}_2}$ ), fol-

lowed by the modifications of cloud optical depth, HNO<sub>3</sub> formation rate via NO<sub>2</sub>+OH,  $\gamma_{\text{N}_2\text{O}_5}$ , and aromatic species emissions. It was also reported in their study that modification of all the parameters could increase the tropospheric NO<sub>2</sub> columns by 18 % during July and by 8 % during Jan-

**Table 5.** Relative changes in the CMAQ-calculated NO<sub>2</sub> columns for several case studies, compared to those from the standard case simulation (Case 1).

Case	Sensitivity test	Season	Relative change <sup>a</sup> (%)							
			CEC	CEC2	SC	SB	SK	JP1	JP2	DM
2	NO <sub>x</sub> seasonal variation (Han et al., 2009)	Spring	33.46	32.44	38.47	32.65	(15.31) <sup>b</sup>	(10.94)	(6.68)	{30.67} <sup>c</sup>
		Summer	-31.16	-28.99	-26.37	-26.42	(-1.40)	(-1.44)	(-1.00)	{-21.96}
		Fall	-21.74	-23.05	-23.90	-21.97	(-2.12)	(-1.20)	(-0.84)	{-18.67}
		Winter	21.25	22.34	22.99	65.37	(12.95)	(8.04)	(7.36)	{23.30}
3	Emission strength (REAS v1.11)	Jan	-32.55	-48.32	-31.45	-58.44	(-0.72)	(27.04)	(-1.02)	{-30.49}
4	γN <sub>2</sub> O <sub>5</sub> (Scheme I: Dentener and Crutzen, 1993) (Scheme II: Riemer et al., 2003) (Scheme IV: Davis et al., 2008) (Scheme V: Brown et al., 2006)	Jan	-9.76	-14.43	-11.71	-7.13	-6.74	-7.51	-4.32	-10.84
		Jan	0.72	-0.54	2.69	4.54	1.91	4.23	2.87	1.52
		Jan	-0.85	-1.60	-1.08	0.04	-0.33	0.37	0.38	-0.87
		Jan	15.59	18.44	22.72	24.76	15.57	14.17	13.02	18.52

<sup>a</sup> Relative change (%) =  $\frac{\Omega_{\text{CASE},i} - \Omega_{\text{CASE},1}}{\Omega_{\text{CASE},1}} \times 100$ , <sup>b</sup>, <sup>c</sup> Since the sensitivity parameters were applied only to China for the case 2 and 3 simulations, the relative changes in the parentheses over the SK, JP1, and JP2 regions indicate indirect impacts caused by long-range transports of the changes from China. The relative changes in the brackets in the entire domain (DM region) also include such indirect impacts from China.

uary. Although the results herein can be complementary to those reported by Lin et al. (2012), all of these issues are ongoing and open questions.

In addition to the issues mentioned above, in the CTM simulations there are additional uncertainties in biological NO<sub>x</sub> emissions from soil and pyrogenic NO<sub>x</sub> emissions (e.g., biomass burning NO<sub>x</sub> emissions) (Bertram et al., 2005; Jaeglé et al., 2005; Hudman et al., 2010; Lin, 2012). However, for example, the biological NO<sub>x</sub> emissions from soil are usually more active during the summer. During the summer, the NO<sub>x</sub> loss rates are so fast that considerations of additional NO<sub>x</sub> emissions would hardly change the CTM-calculated NO<sub>2</sub> columns (Boersma et al., 2009; Han et al., 2009). The same is true for the issues of OH recycling and isoprene-derived alkyl nitrate formation mentioned above. There are uncertainties and unknown chemistry related to isoprene, but, due to the fast NO<sub>x</sub> loss rates during the summer, it has been found that these factors do not greatly affect the  $\Omega_{\text{CMAQ,AK}}$  during the summer in our test runs (data not shown).

On the other hand, in the view of satellite observations, there are errors and uncertainties in the retrievals of the NO<sub>2</sub> vertical columns and the AKs. There are also several NO<sub>2</sub> vertical column products from different sensors (e.g., GOME, OMI, SCIAMACHY, and GOME-2) and from different algorithms (e.g., KNMI, Bremen, BIRA, Harvard Smithsonian, and NASA). For example, the different NO<sub>2</sub> products sometimes show considerable differences (Herron-Thorpe et al., 2010). Overall, different combinations of these sensors and algorithms can produce different NO<sub>2</sub> column products. Thus, in this type of comparison analysis, all the uncertainty factors mentioned above should be taken into account cautiously.

#### 4 Summary and conclusions

The accuracy of bottom-up NO<sub>x</sub> emission fluxes from the INTEX-B, CAPSS, and REAS emission inventories were investigated through comparisons between the  $\Omega_{\text{CMAQ,AK}}$  and

$\Omega_{\text{OMI}}$  in East Asia. For the comparison study, the CMAQ model simulations were carried out over 12 months in 2006 over East Asia. Also, for the direct comparison between the  $\Omega_{\text{CMAQ}}$  and  $\Omega_{\text{OMI}}$ , we applied the AKs to the CMAQ model simulations. This study showed that the seasonal and regional/spatial characteristics from the OMI observations were captured well by the CMAQ model simulations using the INTEX-B, CAPSS, and REAS v1.11 emission inventories over East Asia. It was also found that the normalized mean errors (NMEs) between the  $\Omega_{\text{CMAQ,AK}}$  and  $\Omega_{\text{OMI}}$  for the data from East Asia decreased, from  $\sim 80$  to  $\sim 46$  %, from  $\sim 79$  to  $\sim 44$  %, and from  $\sim 98$  to  $\sim 40$  % during the spring, fall, and winter, respectively, compared with the NME between the  $\Omega_{\text{CMAQ}}$  and  $\Omega_{\text{OMI}}$  (without AKs application). Overall, the  $\Omega_{\text{CMAQ,AK}}$  were an annual average of  $\sim 28$  % (in terms of the NMB; from 7 to 60 % with seasonal variation) smaller in East Asia than the  $\Omega_{\text{OMI}}$ , indicating possible underestimations of the NO<sub>x</sub> emissions used in this study.

To assess the seasonal and spatial discrepancies, several sensitivity studies, shown in Table 1, were performed considering several uncertainty factors such as (i) monthly variation of NO<sub>x</sub> emission, (ii) influences of different NO<sub>x</sub> emissions in East Asia, and (iii) reaction probabilities of N<sub>2</sub>O<sub>5</sub>. In Table 5, we summarize the relative changes in the NO<sub>2</sub> columns from the sensitivity simulations with respect to those from the standard simulation (Case 1). From the sensitivity simulations, we found the following.

- Monthly variations in NO<sub>x</sub> emissions have a strong impact on tropospheric NO<sub>2</sub> columns. The relative changes ranged from -31.16 to 65.37 % over China, when the monthly factors from Han et al. (2009) were used. However, Han et al.'s monthly variations (2009) resulted in even larger discrepancies between  $\Omega_{\text{CMAQ,AK}}$  and  $\Omega_{\text{OMI}}$  over several regions in China. The monthly variations of the INTEX-B NO<sub>x</sub> inventory had a tendency to result in better agreements between the  $\Omega_{\text{CMAQ,AK}}$  and  $\Omega_{\text{OMI}}$  over China.

- As shown in Table 5, when REAS v1.11 inventory data over China were used in the CMAQ model simulations, the  $\Omega_{\text{CMAQ,AK}}$  become  $-31.45$  to  $-58.44$  % lower over China than those from the case with the INTEX-B inventory. Based on this, the NO<sub>x</sub> emissions from the REAS v1.11NO<sub>x</sub> emissions appeared to be more underestimated over China than the INTEX-B NO<sub>x</sub> emissions.
- In the sensitivity test of  $\gamma_{\text{N}_2\text{O}_5}$ , it appeared that the  $\gamma_{\text{N}_2\text{O}_5}$  parameterization would not be a negligible factor, particularly during the winter. The  $\Omega_{\text{CMAQ,AK}}$  from Brown et al.'s (2006) parameterization were  $\sim 19$  % larger over East Asia than the  $\Omega_{\text{CMAQ,AK}}$  from the combined parameterization of Riemer et al. (2003) and Evans and Jacob (2006). In this study, the conventional  $\gamma_{\text{N}_2\text{O}_5}$  parameterizations (Schemes II, III, and IV) showed almost no practical differences in the  $\Omega_{\text{CMAQ,AK}}$  and tended to produce better  $\Omega_{\text{CMAQ,AK}}$  data over East Asia than Schemes I and V.

One of the main driving forces of this study was to correct our previous conclusions (Han et al., 2011), in which AKs were not employed for the comparison between the  $\Omega_{\text{OMI}}$  and  $\Omega_{\text{CMAQ}}$ . Again, this study indicated that the bottom-up NO<sub>x</sub> emissions of the INTEX-B, CAPSS, and REAS v1.11 inventories used in the CMAQ model simulations would be rather underestimated over East Asia. In the sensitivity studies, the influences of different NO<sub>x</sub> emissions and monthly variation in NO<sub>x</sub> emissions can also significantly influence the levels of the  $\Omega_{\text{CMAQ,AK}}$  in East Asia. Moreover, we showed that the  $\gamma_{\text{N}_2\text{O}_5}$  parameterization could be another important factor in the winter. Because other possible uncertainty factors still exist, as discussed in Sect. 3.2.4, further analyses are definitely necessary in future studies.

The estimation of “top-down” NO<sub>x</sub> emissions has also been carried out in East Asia (Stavrakou et al., 2008; Lin et al., 2010; Mijling et al., 2013) using satellite-derived NO<sub>2</sub> columns. However, in such top-down estimations, other uncertain (limiting) factors exist, such as the lifetime of NO<sub>x</sub> (i.e.,  $\tau_{\text{NO}_x}$ ). The uncertainty in  $\tau_{\text{NO}_x}$  is also linked with the factors discussed herein in Sect. 3.2.4. In addition, even in the top-down NO<sub>x</sub> emission, the random and smoothing errors should be reduced/minimized via temporal and/or spatial averaging and the application of AKs, respectively, as demonstrated herein.

Improvements in the NO<sub>x</sub> emissions data or evaluation of the accuracy of bottom-up NO<sub>x</sub> emission fluxes in East Asia can improve air quality modeling and chemical weather forecasting over East Asia. Thus, much effort should be focused on this issue in the future, particularly on the circumstances over East Asia. In this context, efforts in inverse modeling to improve the NO<sub>x</sub> emissions data over East Asia, such as adjoint modeling with measured data and top-down estimations of the NO<sub>x</sub> emissions with satellite observations, could also contribute to improving the performance of air quality modeling and the accuracy of chemical weather forecasting over East Asia (Park et al., 2013).

## Appendix A

For statistical analyses between the CMAQ-calculated and OMI-retrieved tropospheric NO<sub>2</sub> columns, several statistical parameters below are introduced in Table A1.

1. Absolute errors and biases: the mean error (ME) and the mean bias (MB) are statistical parameters used to measure how close the estimated values ( $\Omega_{\text{CMAQ,AK}}$  in this study) are to the observed values ( $\Omega_{\text{OMI}}$  in this study). The distinction between the two parameters is that the MB provides information on overestimation (i.e., positive values) or underestimation (i.e., negative values) of the estimated values.
2. Relative errors and biases: the mean normalized gross error (MNGE) and the mean normalized bias (MNB) are statistical parameters used to measure the relative differences normalized by the observed values. The values of the MNGE and MNB can be significantly inflated (or overstated), when observations are sometimes close to zero. In this case, the normalized mean error (NME) and the normalized mean bias (NMB) can be useful statistical parameters, because they avoid over-inflating the measured range. However, these bias parameters have an issue of asymmetry, meaning that overestimations (i.e.,  $+\infty$ ) are weighted more than the equivalent underestimations (i.e.,  $-100$ ), as shown in Table A1. The mean fractional bias (MFB) provides equal weight to both sides, which range from  $-200$  to  $+200$ , as shown in Table A1.
3. Agreements: the Pearson correlation coefficient ( $R$ ) is a statistical parameter to measure the degree to which both the estimated and observed values are linearly related. The value of  $R = 1$  indicates perfect agreement between both values, whereas  $R = 0$  means no linear relationship. The Pearson correlation coefficient can sometimes be numerically unstable, depending on the sample size. The index of agreement (IOA) is a standardized measure of the degree of estimation error, ranging from 0 to 1 (Willmott, 1981). Unlike the Pearson correlation coefficient, the IOA can account for additive and proportional differences in the estimated and observed means and variances. The value of 0 indicates no agreement between the estimated and observed values, whereas the value of 1 indicates perfect agreement.

**Table A1.** Statistical parameters used in this study.

Parameters (unit)	Equations *	Range
Mean error (molecules cm <sup>-2</sup> )	$ME = \frac{1}{N} \sum_{i=1}^N  \Omega_{\text{CMAQ,AK}} - \Omega_{\text{OMI}} $	0 to +∞
Mean bias (molecules cm <sup>-2</sup> )	$MB = \frac{1}{N} \sum_{i=1}^N (\Omega_{\text{CMAQ,AK}} - \Omega_{\text{OMI}}) = \overline{\Omega_{\text{CMAQ,AK}}} - \overline{\Omega_{\text{OMI}}}$	$-\overline{\Omega_{\text{OMI}}}$ to +∞
Mean normalized gross error (%)	$MNGE = \frac{1}{N} \sum_{i=1}^N \frac{ \Omega_{\text{CMAQ,AK}} - \Omega_{\text{OMI}} }{\Omega_{\text{OMI}}} \times 100$	0 to +∞
Mean normalized bias (%)	$MNB = \frac{1}{N} \sum_{i=1}^N \left( \frac{\Omega_{\text{CMAQ,AK}} - \Omega_{\text{OMI}}}{\Omega_{\text{OMI}}} \right) \times 100$	-100 to +∞
Normalized mean error (%)	$NME = \frac{\sum_{i=1}^N  \Omega_{\text{CMAQ,AK}} - \Omega_{\text{OMI}} }{\sum_{i=1}^N \Omega_{\text{OMI}}} \times 100$	0 to +∞
Normalized mean bias (%)	$NMB = \frac{\sum_{i=1}^N (\Omega_{\text{CMAQ,AK}} - \Omega_{\text{OMI}})}{\sum_{i=1}^N \Omega_{\text{OMI}}} \times 100$	-100 to +∞
Mean fractional error (%)	$MFE = \frac{1}{N} \sum_{i=1}^N \frac{ \Omega_{\text{CMAQ,AK}} - \Omega_{\text{OMI}} }{\left( \frac{\Omega_{\text{CMAQ,AK}} + \Omega_{\text{OMI}}}{2} \right)} \times 100$	0 to +200
Mean fractional bias (%)	$MFB = \frac{1}{N} \sum_{i=1}^N \frac{(\Omega_{\text{CMAQ,AK}} - \Omega_{\text{OMI}})}{\left( \frac{\Omega_{\text{CMAQ,AK}} + \Omega_{\text{OMI}}}{2} \right)} \times 100$	-200 to +200
Pearson correlation coefficient (dimensionless)	$R = \frac{\sum_{i=1}^N (\Omega_{\text{CMAQ,AK}} - \overline{\Omega_{\text{CMAQ,AK}}})(\Omega_{\text{OMI}} - \overline{\Omega_{\text{OMI}}})}{\sqrt{\sum_{i=1}^N (\Omega_{\text{CMAQ,AK}} - \overline{\Omega_{\text{CMAQ,AK}}})^2 \sum_{i=1}^N (\Omega_{\text{OMI}} - \overline{\Omega_{\text{OMI}}})^2}}$	-1 to +1
Index of agreement (dimensionless)	$IOA = 1 - \frac{\sum_{i=1}^N (\Omega_{\text{CMAQ,AK}} - \Omega_{\text{OMI}})^2}{\sum_{i=1}^N ( \Omega_{\text{CMAQ,AK}} - \overline{\Omega_{\text{OMI}}}  +  \Omega_{\text{OMI}} - \overline{\Omega_{\text{OMI}}} )^2}$	0 to +1

\* $\Omega_{\text{CMAQ,AK}}$  and  $\Omega_{\text{OMI}}$  indicate the CMAQ-calculated NO<sub>2</sub> columns with the consideration of AKs and the OMI-retrieved NO<sub>2</sub> columns, respectively.  $N$  represents the number of data samples.

The Supplement related to this article is available online at doi:10.5194/acp-15-1913-2015-supplement.

*Acknowledgements.* This research was supported by the GEMS program of the Ministry of Environment, South Korea, as part of the Eco Innovation Program of KEITI (2012000160004). This work was also supported by the Basic Science Research Program through the National Research Foundation of Korea (NRF), funded by the Ministry of Science, ICT & Future Planning (2014R1A1A1004523), and by the Korea Meteorological Administration Research and Development Program under Grant CATER 2012-7110. We would like to acknowledge the use of the tropospheric NO<sub>2</sub> column data from <http://www.temis.nl>.

Edited by: G. Frost

## References

- Archibald, A. T., Cooke, M. C., Utembe, S. R., Shallcross, D. E., Derwent, R. G., and Jenkin, M. E.: Impacts of mechanistic changes on HO<sub>x</sub> formation and recycling in the oxidation of isoprene, *Atmos. Chem. Phys.*, 10, 8097–8118, doi:10.5194/acp-10-8097-2010, 2010.
- Atkinson, R., Baulch, D. L., Cox, R. A., Crowley, J. N., Hampson, R. F., Hynes, R. G., Jenkin, M. E., Rossi, M. J., and Troe, J.: Evaluated kinetic and photochemical data for atmospheric chemistry: Volume I - gas phase reactions of O<sub>x</sub>, HO<sub>x</sub>, NO<sub>x</sub> and SO<sub>x</sub> species, *Atmos. Chem. Phys.*, 4, 1461–1738, doi:10.5194/acp-4-1461-2004, 2004.
- Bertram, T. H., Heckel, A., Richter, A., Burrows, J. P., and Cohen, R. C.: Satellite measurements of daily variations in soil NO<sub>x</sub> emissions, *Geophys. Res. Lett.*, 32, L24812, doi:10.1029/2005GL024640, 2005.
- Bertram, T. H., Thornton, J. A., Riedel, T. P., Middlebrook, A. M., Bahreini, R., Bates, T. S., Quinn, P. K., and Coffman, D. J.: Direct observations of N<sub>2</sub>O<sub>5</sub> reactivity on ambient aerosol particles, *Geophys. Res. Lett.*, 36, L19803, doi:10.1029/2009GL040248, 2009.
- Binkowski, F. S. and Roselle, S. J.: Models-3 Community Multi-scale Air Quality (CMAQ) model aerosol components: 1. model description, *J. Geophys. Res.*, 108, 4183, doi:10.1029/2001JD001409, 2003.
- Boersma, K. F., Eskes, H. J., Veeffkind, J. P., Brinksma, E. J., van der A, R. J., Sneep, M., van den Oord, G. H. J., Levelt, P. F., Stammes, P., Gleason, J. F., and Bucsela, E. J.: Near-real time retrieval of tropospheric NO<sub>2</sub> from OMI, *Atmos. Chem. Phys.*, 7, 2103–2118, doi:10.5194/acp-7-2103-2007, 2007.
- Boersma, K. F., Jacob, D. J., Trainic, M., Rudich, Y., DeSmedt, I., Dirksen, R., and Eskes, H. J.: Validation of urban NO<sub>2</sub> concentrations and their diurnal and seasonal variations observed from the SCIAMACHY and OMI sensors using in situ surface measurements in Israeli cities, *Atmos. Chem. Phys.*, 9, 3867–3879, doi:10.5194/acp-9-3867-2009, 2009.
- Boersma, K. F., Eskes, H. J., Dirksen, R. J., van der A, R. J., Veeffkind, J. P., Stammes, P., Huijnen, V., Kleipool, Q. L., Sneep, M., Claas, J., Leitão, J., Richter, A., Zhou, Y., and Brunner, D.: An improved tropospheric NO<sub>2</sub> column retrieval algorithm for the Ozone Monitoring Instrument, *Atmos. Meas. Tech.*, 4, 1905–1928, doi:10.5194/amt-4-1905-2011, 2011a.
- Boersma, K. F., Braak, R., and van der A, R. J.: Dutch OMI NO<sub>2</sub> (DOMINO) data product v2.0 HE5 data file user manual, TEMIS website, available at: <http://www.temis.nl/airpollution/no2.html> (last access: 2 October 2014), 2011b.
- Brown, S. S., Dibb, J. E., Stark, H., Aldener, M., Vozella, M., Whitlow, S., Williams, E. J., Lerner, B. M., Jakoubek, R., Middlebrook, A. M., DeGouw, J. A., Warneke, C., Goldan, P. D., Kuster, W. C., Angevine, W. M., Sueper, D. T., Quinn P. K., Bates, T. S., Meagher, J. F., Fehsenfeld, F. C., and Ravishankara, A. R.: Night-time removal of NO<sub>x</sub> in the summer marine boundary layer, *Geophys. Res. Lett.*, 31, L07108, doi:10.1029/2004GL019412, 2004.
- Brown, S. S., Ryerson, T. B., Wollny, A. G., Brock, C. A., Peltier, R., Sullivan, A. P., Weber, R. J., Dube, W. P., Trainer, M., Meagher, J. F., Fehsenfeld, F. C., and Ravishankara, A. R.: Variability in nocturnal nitrogen oxide processing and its role in regional air quality, *Science*, 311, 67–70, 2006.
- Brown, S. S., Dubé, W. P., Fuchs, H., Ryerson, T. B., Wollny, A. G., Brock, C. A., Bahreini, R., Middlebrook, A. M., Neuman, J. A., Atlas, E., Roberts, J. M., Osthoff, H. D., Trainer, M., Fehsenfeld, F. C., and Ravishankara, A. R.: Reactive Uptake Coefficients for N<sub>2</sub>O<sub>5</sub> Determined from Aircraft Measurements during the Second Texas Air Quality Study: Comparison to Current Model Parameterizations, *J. Geophys. Res.* 114, D00F10, doi:10.1029/2008JD011679, 2009.
- Browne, E. C. and Cohen, R. C.: Effects of biogenic nitrate chemistry on the NO<sub>x</sub> lifetime in remote continental regions, *Atmos. Chem. Phys.*, 12, 11917–11932, doi:10.5194/acp-12-11917-2012, 2012.
- Browne, E. C., Min, K.-E., Wooldridge, P. J., Apel, E., Blake, D. R., Brune, W. H., Cantrell, C. A., Cubison, M. J., Diskin, G. S., Jimenez, J. L., Weinheimer, A. J., Wennberg, P. O., Wisthaler, A., and Cohen, R. C.: Observations of total RONO<sub>2</sub> over the boreal forest: NO<sub>x</sub> sinks and HNO<sub>3</sub> sources, *Atmos. Chem. Phys.*, 13, 4543–4562, doi:10.5194/acp-13-4543-2013, 2013.
- Butkovskaya, N. I., Kukui, A., Pouvesle, N., and Le Bras, G.: Formation of Nitric Acid in the Gas-Phase HO<sub>2</sub>+ NO Reaction: Effects of Temperature and Water Vapor, *J. Phys. Chem. A*, 109, 6509–6520, doi:10.1021/jp051534v, 2005.
- Butkovskaya, N., Rayez, M.-T., Rayez, J.-C., Kukui, A., and Le Bras, G.: Water vapor effect on the HNO<sub>3</sub> yield in the HO<sub>2</sub>+ NO reaction: Experimental and theoretical evidence, *J. Phys. Chem. A*, 113, 11327–11342, doi:10.1021/jp811428p, 2009.
- Butler, T. M., Taraborrelli, D., Brühl, C., Fischer, H., Harder, H., Martinez, M., Williams, J., Lawrence, M. G., and Lelieveld, J.: Improved simulation of isoprene oxidation chemistry with the ECHAM5/MESy chemistry-climate model: lessons from the GABRIEL airborne field campaign, *Atmos. Chem. Phys.*, 8, 4529–4546, doi:10.5194/acp-8-4529-2008, 2008.
- Byun, D. W. and Schere, K. L.: Review of the governing equations, computational algorithm, and other components of the Models-3 Community Multi-scale Air Quality (CMAQ) Modeling system, *Appl. Mech. Rev.*, 59, 51–77, 2006.

- Carter, W. P. L.: Implementation of the SAPRC-99 Chemical Mechanism into the Models-3 Framework, Report to the United States Environmental Protection Agency, available at: <http://www.engr.ucr.edu/~carter/pubs/s99mod3.pdf> (last access: 6 February 2015), 2000.
- Clarisse, L., Coheur, P.-F., Prata, F., Hadji-Lazaro, J., Hurtmans, D., and Clerbaux, C.: A unified approach to infrared aerosol remote sensing and type specification, *Atmos. Chem. Phys.*, 13, 2195–2221, doi:10.5194/acp-13-2195-2013, 2013.
- Cofala, J., Bertok, I., Borken-Kleefeld, J., Heyes, C., Klimont, Z., Rafaj, P., Sander, R., Schöpp, W., and Amann, M.: Emissions of Air Pollutants for the World Energy Outlook 2012 Energy Scenarios, International Institute for Applied System Analysis (IIASA), 2361, Laxenburg, Austria, available at: [http://www.iiasa.ac.at/publication/more\\_XO-12-020.php](http://www.iiasa.ac.at/publication/more_XO-12-020.php) (last access: 6 February 2015), 2012.
- Davis, J. M., Bhave, P. V., and Foley, K. M.: Parameterization of N<sub>2</sub>O<sub>5</sub> reaction probabilities on the surface of particles containing ammonium, sulfate, and nitrate, *Atmos. Chem. Phys.*, 8, 5295–5311, doi:10.5194/acp-8-5295-2008, 2008.
- Dentener, F. J. and Crutzen, P. J.: Reaction of N<sub>2</sub>O<sub>5</sub> on tropospheric aerosols: Impact on the global distribution of NO<sub>x</sub>, O<sub>3</sub>, and OH levels, *J. Geophys. Res.*, 98, 7149–7163, 1993.
- Emmons, L. K., Walters, S., Hess, P. G., Lamarque, J.-F., Pfister, G. G., Fillmore, D., Granier, C., Guenther, A., Kinnison, D., Laepple, T., Orlando, J., Tie, X., Tyndall, G., Wiedinmyer, C., Baughcum, S. L., and Kloster, S.: Description and evaluation of the Model for Ozone and Related chemical Tracers, version 4 (MOZART-4), *Geosci. Model Dev.*, 3, 43–67, doi:10.5194/gmd-3-43-2010, 2010.
- Eskes, H. J. and Boersma, K. F.: Averaging kernels for DOAS total-column satellite retrievals, *Atmos. Chem. Phys.*, 3, 1285–1291, doi:10.5194/acp-3-1285-2003, 2003.
- Evans, M. J. and Jacob, D. J.: Impact of new laboratory studies of N<sub>2</sub>O<sub>5</sub> hydrolysis on global model budgets of tropospheric nitrogen oxides, ozone, and OH, *Geophys. Res. Lett.*, 32, L09813, doi:10.1029/2005GL022469, 2005.
- Fioletov, V. E., Bodeker, G. E., Miller, A. J., McPeters, R. D., and Stolarski, R.: Global and zonal total ozone variations estimated from ground-based and satellite measurements: 1964–2000, *J. Geophys. Res.*, 107, 4647, doi:10.1029/2001JD001350, 2002.
- Fu, T., Jacob, D. J., Palmer, P. I., Chance, K., Wang, Y. X., Barletta, B., Blake, D. R., Staton, J. C., and Pilling, M. J.: Space-based formaldehyde measurements as constraints on volatile organic compound emissions in east and south Asia and implications for ozone, *J. Geophys. Res.*, 112, D06312, doi:10.1029/2006JD007853, 2007.
- Ghude, S. D., Pfister, G. G., Jena, C., van der A, R. J., Emmons, L. K., and Kumar, R.: Satellite constraints of nitrogen oxide (NO<sub>x</sub>) emissions from India based on OMI observations and WRF-Chem simulations, *Geophys. Res. Lett.*, 40, 1–6, doi:10.1029/2012GL053926, 2013.
- Han, K. M., Song, C. H., Ahn, H. J., Park, R. S., Woo, J. H., Lee, C. K., Richter, A., Burrows, J. P., Kim, J. Y., and Hong, J. H.: Investigation of NO<sub>x</sub> emissions and NO<sub>x</sub>-related chemistry in East Asia using CMAQ-predicted and GOME-derived NO<sub>2</sub> columns, *Atmos. Chem. Phys.*, 9, 1017–1036, doi:10.5194/acp-9-1017-2009, 2009.
- Han, K. M., Lee, C. K., Lee, J., Kim, J., and Song, C. H.: A comparison study between model-predicted and OMI-retrieved tropospheric NO<sub>2</sub> columns over the Korean peninsula, *Atmos. Environ.*, 45, 2962–2971, 2011.
- Han, K. M. and Song, C. H.: A budget analysis of NO<sub>x</sub> column losses over the Korean peninsula, *Asia-Pacific J. Atmos. Sci.*, 48, 55–65, 2012.
- Han, K. M., Park, R. S., Kim, H. K., Woo, J. H., Kim, J., and Song, C. H.: Uncertainty in biogenic isoprene emissions and its impacts on tropospheric chemistry in East Asia, *Sci. Total Environ.*, 463, 754–771, 2013.
- Harris, G. W., Carter, W. P. L., Winer, A. M., Pitts, J. N., Platt, U., and Perner, D.: Observations of nitrous acid in the Los Angeles atmosphere and implications for predictions of ozone-precursor relationships, *Environ. Sci. Technol.*, 16, 414–419, doi:10.1021/es00101a009, 1982.
- He, Y., Uno, I., Wang, Z., Ohara, T., Sugimoto, N., Shimizu, A., Richter, A., and Burrows, J. P.: Variations of the increasing trend of tropospheric NO<sub>2</sub> over central east China during the past decade, *Atmos. Environ.*, 41, 4865–4876, 2007.
- Henderson, B. H., Pinder, R. W., Crooks, J., Cohen, R. C., Carlton, A. G., Pye, H. O. T., and Vizuete, W.: Combining Bayesian methods and aircraft observations to constrain the HO<sub>2</sub> + NO<sub>2</sub> reaction rate, *Atmos. Chem. Phys.*, 12, 653–667, doi:10.5194/acp-12-653-2012, 2012.
- Herron-Thorpe, F. L., Lamb, B. K., Mount, G. H., and Vaughan, J. K.: Evaluation of a regional air quality forecast model for tropospheric NO<sub>2</sub> columns using the OMI/Aura satellite tropospheric NO<sub>2</sub> product, *Atmos. Chem. Phys.*, 10, 8839–8854, doi:10.5194/acp-10-8839-2010, 2010.
- Hilboll, A., Richter, A., and Burrows, J. P.: Long-term changes of tropospheric NO<sub>2</sub> over megacities derived from multiple satellite instruments, *Atmos. Chem. Phys.*, 13, 4145–4169, doi:10.5194/acp-13-4145-2013, 2013.
- Hong, J. H., Lee, W. S., Kim, D. G., Lee, S. B., Kang, K. H.: 2006 Greenhouse gas and air pollutants emissions in Korea, National Institute of Environmental Research (NIER), Ministry of Environment of Korea, available at: <http://airemiss.nier.go.kr/upload2/data/airpollution/62.pdf> (last access: 6 February 2015), 2008.
- Horowitz, L., Fiore, A. M., Milly, G. P., Cohen, R. C., Perring, A., Wooldridge, P. J., Hess, P. G., Emmons, L. K., and Lamarque, J.-F.: Observational constraints on the chemistry of isoprene nitrates over the eastern United States, *J. Geophys. Res.*, 112, D12S08, doi:10.1029/2006JD007747, 2007.
- Hudman, R. C., Russell, A. R., Valin, L. C., and Cohen, R. C.: Interannual variability in soil nitric oxide emissions over the United States as viewed from space, *Atmos. Chem. Phys.*, 10, 9943–9952, doi:10.5194/acp-10-9943-2010, 2010.
- Huijnen, V., Eskes, H. J., Poupkou, A., Elbern, H., Boersma, K. F., Foret, G., Sofiev, M., Valdebenito, A., Flemming, J., Stein, O., Gross, A., Robertson, L., D'Isidoro, M., Kioutsioukis, I., Friese, E., Amstrup, B., Bergstrom, R., Strunk, A., Virá, J., Zyryanov, D., Maurizi, A., Melas, D., Peuch, V.-H., and Zerefos, C.: Comparison of OMI NO<sub>2</sub> tropospheric columns with an ensemble of global and European regional air quality models, *Atmos. Chem. Phys.*, 10, 3273–3296, doi:10.5194/acp-10-3273-2010, 2010.
- Itahashi, S., Uno, I., Irie, H., Kurokawa, J.-I., and Ohara, T.: Regional modeling of tropospheric NO<sub>2</sub> vertical column density

- over East Asia during the period 2000–2010: comparison with multisatellite observations, *Atmos. Chem. Phys.*, 14, 3623–3635, doi:10.5194/acp-14-3623-2014, 2014.
- Jacob, D. J.: Heterogeneous chemistry and tropospheric ozone, *Atmos. Environ.*, 34, 2131–2159, 2000.
- Jaeglé, L., Steinberger, L., Martin, R. V., and Chance, K.: Global partitioning of NO<sub>x</sub> sources using satellite observations: Relative roles of fossil fuel combustion, biomass burning and soil emissions, *Faraday Discuss.*, 130, 407–423, doi:10.1039/b502128f, 2005.
- Johnson, E. S., Bonjean, F., Lagerloef, G. S. E., and Gunn, J. T.: Validation and error analysis of OSCAR sea surface currents, *J. Atmos. Oceanic Technol.*, 24, 688–701, 2007.
- Karamchandani, P., Santos, L., Sykes, I., Zhang, Y., Tonne, C., and Seigneur, C.: Development and evaluation of a state-of-the-science reactive plume model, *Environ. Sci. Technol.*, 34, 870–880, 2000.
- Kim, J.: GEMS (Geostationary Environment Monitoring Spectrometer) onboard the GeoKOMPSAT to Monitor Air Quality in high Temporal and Spatial Resolution over Asia-Pacific Region, EGU General Assembly 2012, 22–27 April 2012, Vienna, Austria, p. 4051, 2012.
- Kim, H. S., Song, C. H., Park, R. S., Huey, G., and Ryu, J. Y.: Investigation of ship-plume chemistry using a newly-developed photochemical/dynamic ship-plume model, *Atmos. Chem. Phys.*, 9, 7531–7550, doi:10.5194/acp-9-7531-2009, 2009.
- Kleipool, Q. L., Dobber, M. R., de Haan, J. F., and Levelt, P. E.: Earth surface reflectance climatology from 3 years of OMI data, *J. Geophys. Res.*, 113, D18308, doi:10.1029/2008JD010290, 2008.
- Klimont, Z., Cofala, J., Xing, J., Wei, W., Zhang, C., Wang, S., Kejun, J., Bhandari, P., Mathur, R., Purohit, P., Rafaj, P., Chambers, A., Amann, M., and Hao, J.: Projections of SO<sub>2</sub>, NO<sub>x</sub>, and carbonaceous aerosols emissions in Asia, *Tellus*, 61, 602–617, 2009.
- Kubistin, D., Harder, H., Martinez, M., Rudolf, M., Sander, R., Bozem, H., Eerdeken, G., Fischer, H., Gurk, C., Klüpfel, T., Königstedt, R., Parchatka, U., Schiller, C. L., Stickler, A., Taraborrelli, D., Williams, J., and Lelieveld, J.: Hydroxyl radicals in the tropical troposphere over the Suriname rainforest: comparison of measurements with the box model MECCA, *Atmos. Chem. Phys.*, 10, 9705–9728, doi:10.5194/acp-10-9705-2010, 2010.
- Kurokawa, J., Ohara, T., Morikawa, T., Hanayama, S., Janssens-Maenhout, G., Fukui, T., Kawashima, K., and Akimoto, H.: Emissions of air pollutants and greenhouse gases over Asian regions during 2000–2008: Regional Emission inventory in ASIA (REAS) version 2, *Atmos. Chem. Phys.*, 13, 11019–11058, doi:10.5194/acp-13-11019-2013, 2013.
- Lamsal, L. N., Martin, R. V., van Donkelaar, A., Celarier, E. A., Bucsela, E. J., Boersma, K. F., Dirksen, R., Luo, C., and Wang, Y.: Indirect validation of tropospheric nitrogen dioxide retrieved from the OMI satellite instrument: Insight into the seasonal variation of nitrogen oxides at northern midlatitudes, *J. Geophys. Res.*, 115, D05302, doi:10.1029/2009JD013351, 2010.
- Lelieveld, J., Butler, T. M., Crowley, J. N., Dillon, T. J., Fischer, H., Ganzeveld, L., Harder, H., Lawrence, M. G., Martinez, M., Taraborrelli, D., and Williams, J.: Atmospheric oxidation capacity sustained by a tropical forest, *Nature*, 452, 737–740, doi:10.1038/nature06870, 2008.
- Levelt, P. F., van den Oord, G. H. J., Dobber, M. R., Mälkki, A., Visser, H., de Vries, J., Stammes, P., Lundell, J. O. V., and Saari, H.: The Ozone Monitoring Instrument, *IEEE Trans. Geosci. Remote Sens.*, 44, 1093–1101, 2006.
- Lin, J.-T., McElroy, M. B., and Boersma, K. F.: Constraint of anthropogenic NO<sub>x</sub> emissions in China from different sectors: a new methodology using multiple satellite retrievals, *Atmos. Chem. Phys.*, 10, 63–78, doi:10.5194/acp-10-63-2010, 2010.
- Lin, J.-T.: Satellite constraint for emissions of nitrogen oxides from anthropogenic, lightning and soil sources over East China on a high-resolution grid, *Atmos. Chem. Phys.*, 12, 2881–2898, doi:10.5194/acp-12-2881-2012, 2012.
- Lin, J.-T., Liu, Z., Zhang, Q., Liu, H., Mao, J., and Zhuang, G.: Modeling uncertainties for tropospheric nitrogen dioxide columns affecting satellite-based inverse modeling of nitrogen oxides emissions, *Atmos. Chem. Phys.*, 12, 12255–12275, doi:10.5194/acp-12-12255-2012, 2012.
- Ma, J., Richter, A., Burrows, J. P., Nüß, H., and van Aardenne, J. A.: Comparison of model-simulated tropospheric NO<sub>2</sub> over China with GOME-satellite data, *Atmos. Environ.*, 40, 593–604, 2006.
- Macintyre, H. L. and Evans, M. J.: Sensitivity of a global model to the uptake of N<sub>2</sub>O<sub>5</sub> by tropospheric aerosol, *Atmos. Chem. Phys.*, 10, 7409–7414, doi:10.5194/acp-10-7409-2010, 2010.
- Martin, R. V., Sioris, C. E., Chance, K., Ryerson, T. B., Bertram, T. H., Wooldridge, P. J., Cohen, R. C., Neuman, J. A., Swanson, A., and Flocke, F. M.: Evaluation of space-based constraints on global nitrogen oxide emissions with regional aircraft measurements over and downwind of eastern North America, *J. Geophys. Res.*, 111, D15308, doi:10.1029/2005JD006680, 2006.
- McConnell, J. C. and McElroy, M. B.: Odd nitrogen in the atmosphere, *J. Atmos. Sci.*, 30, 1465–1480, 1973.
- Mijling, B., van der A, R. J., and Zhang, Q.: Regional nitrogen oxides emission trends in East Asia observed from space, *Atmos. Chem. Phys.*, 13, 12003–12012, doi:10.5194/acp-13-12003-2013, 2013.
- Möllner, A. K., Valluvadasan, S., Feng, L., Sprague, M. K., Okumura, M., Milligan, D. B., Bloss, W. J., Sander, S. P., Martien, P. T., Harley, R. A., McCoy, A. B., and Carter, W. P. L.: Rate of Gas Phase Association of Hydroxyl Radical and Nitrogen Dioxide, *Science*, 330, 646–649, doi:10.1126/science.1193030, 2010.
- Monaghan, A. J., Bromwich, D. H., and Wang, S. H.: Recent trends in Antarctic snow accumulation from Polar MM5 simulations, *Phil. Trans. R. Soc. A*, 364, 1683–1708, doi:10.1098/rsta.2006.1795, 2006.
- Müller, J.-F., Stavrakou, T., Wallens, S., De Smedt, I., Van Roozendaal, M., Potosnak, M. J., Rinne, J., Munger, B., Goldstein, A., and Guenther, A. B.: Global isoprene emissions estimated using MEGAN, ECMWF analyses and a detailed canopy environment model, *Atmos. Chem. Phys.*, 8, 1329–1341, doi:10.5194/acp-8-1329-2008, 2008.
- Ohara, T., Akimoto, H., Kurokawa, J., Horii, N., Yamaji, K., Yan, X., and Hayasaka, T.: An Asian emission inventory of anthropogenic emission sources for the period 1980–2020, *Atmos. Chem. Phys.*, 7, 4419–4444, doi:10.5194/acp-7-4419-2007, 2007.
- Pagsberg, P., Bjergbakke, E., Ratajczak, E., and Silleston, A.: Kinetics of the gas phase reaction OH + NO(+M) → HONO(+M) and the determination of the UV absorption cross sections of HONO, *Chem. Phys. Lett.*, 272, 383–390, 1997.



- Park, R. S., Han, K. M., Song, C. H., Park, M. E., Lee, S. J., Hong, S. Y., Kim, J., and Woo, J.-H.: Current Status and Development of Modeling Techniques for Forecasting and Monitoring of Air Quality over East Asia, *J. KOSAE*, 29, 407–438, 2013 (in Korean).
- Park, R. S., Lee, S., Shin, S.-K., and Song, C. H.: Contribution of ammonium nitrate to aerosol optical depth and direct radiative forcing by aerosols over East Asia, *Atmos. Chem. Phys.*, 14, 2185–2201, doi:10.5194/acp-14-2185-2014, 2014.
- Platt, U. F., Winer, A. M., Biermann, H. W., Atkinson, R., and Pitts, J. N.: Measurement of nitrate radical concentrations in continental air, *Environ. Sci. Technol.*, 18, 365–369, doi:10.1021/es00123a015, 1984.
- Pleim, J. E.: A combined local and nonlocal closure model for the atmospheric boundary layer, Part I: Model description and testing, *J. Appl. Meteor. Climatol.*, 46, 1383–1395, 2007.
- Pugh, T. A. M., MacKenzie, A. R., Hewitt, C. N., Langford, B., Edwards, P. M., Furneaux, K. L., Heard, D. E., Hopkins, J. R., Jones, C. E., Karunaharan, A., Lee, J., Mills, G., Misztal, P., Moller, S., Monks, P. S., and Whalley, L. K.: Simulating atmospheric composition over a South-East Asian tropical rainforest: performance of a chemistry box model, *Atmos. Chem. Phys.*, 10, 279–298, doi:10.5194/acp-10-279-2010, 2010.
- Richter, A., Burrows, J. P., Nüß, H., Granier, C., and Niemeier, U.: Increase in tropospheric nitrogen dioxide over China observed from space, *Nature*, 437, 129–132, 2005.
- Richter, A., Begoin, M., Hilboll, A., and Burrows, J. P.: An improved NO<sub>2</sub> retrieval for the GOME-2 satellite instrument, *Atmos. Meas. Tech.*, 4, 1147–1159, doi:10.5194/amt-4-1147-2011, 2011.
- Riemer, N., Vogel, H., Vogel, B., Schell, B., Ackermann, I., Kessler, C., and Hass, H.: Impact of the heterogeneous hydrolysis of N<sub>2</sub>O<sub>5</sub> on chemistry and nitrate aerosol formation in the lower troposphere under photochemical conditions, *J. Geophys. Res.*, 108, 4144, doi:10.1029/2002JD002436, 2003.
- Roberts, J. M., Flocke, F., Stroud, C. A., Hereid, D., Williams, E. J., Fehsenfeld, F. C., Brune, W., Martinez, M., and Harder, H.: Ground-based measurements of peroxyacetylnitric anhydrides (PANs) during the 1999 Southern Oxidant Study Nashville Intensive, *J. Geophys. Res.*, 107, 4554, doi:10.1029/2001JD000947, 2002.
- Rodgers, C. D.: Inverse methods for atmospheric sounding: theory and practice, Series on Atmospheric, Oceanic and Planetary Physics – Vol. 2, World Scientific Publishing, Singapore, 43–63, 2000.
- Rondon, A. and Sanhueza, E.: High HONO atmospheric concentrations during vegetation burning in the tropical savannah, *Tellus B*, 41B, 474–477, doi:10.1111/j.1600-0889.1989.tb00323.x, 1989.
- Sander, S. P., Abbatt, J., Barker, J. R., Burkholder, J. B., Friedl, R. R., Golden, D. M., Huie, R. E., Kolb, C. E., Kurylo, M. J., Moortgat, G. K., Orkin, V. L., and Wine, P. H.: Chemical Kinetics and Photochemical Data for Use in Atmospheric Studies, Evaluation number 17, NASA Panel for data evaluation, JPL Publication 10-6, Jet Propulsion Laboratory, Pasadena, <http://jpldataeval.jpl.nasa.gov> (last access: 27 June 2014), 2011.
- Schneider, P. and van der A, R. J.: A global single-sensor analysis of 2002–2011 tropospheric nitrogen dioxide trends observed from space, *J. Geophys. Res.*, 117, D16309, doi:10.1029/2012JD017571, 2012.
- Shi, C., Fernando, H. J. S., Wang, Z., An, X., and Wu, Q.: Tropospheric NO<sub>2</sub> columns over East Central China: Comparisons between SCIAMACHY measurements and nested CMAQ simulations, *Atmos. Environ.*, 42, 7165–7173, 2008.
- Song, C. H., Chen, G., Hanna, S. R., Crawford, J., and Davis, D. D.: Dispersion and chemical evolution of ship plumes in the marine boundary layer: Investigation of O<sub>3</sub>/NO<sub>y</sub>/HO<sub>x</sub> chemistry, *J. Geophys. Res.*, 108, 4143, doi:10.1029/2002JD002216, 2003.
- Song, C. H., Kim, H. S., von Glasow, R., Brimblecombe, P., Kim, J., Park, R. J., Woo, J. H., and Kim, Y. H.: Source identification and budget analysis on elevated levels of formaldehyde within the ship plumes: a ship-plume photochemical/dynamic model analysis, *Atmos. Chem. Phys.*, 10, 11969–11985, doi:10.5194/acp-10-11969-2010, 2010.
- Sörgel, M., Regelin, E., Bozem, H., Diesch, J.-M., Drewnick, F., Fischer, H., Harder, H., Held, A., Hosaynali-Beygi, Z., Martinez, M., and Zetzsch, C.: Quantification of the unknown HONO daytime source and its relation to NO<sub>2</sub>, *Atmos. Chem. Phys.*, 11, 10433–10447, doi:10.5194/acp-11-10433-2011, 2011.
- Stauffer, D. R. and Seaman, N. L.: Use of four-dimensional data assimilation in a limited-area mesoscale model. Part I: experiments with synoptic-scale data, *Monthly Weather Review*, 118, 1250–1277, 1990.
- Stauffer, D. L. and Seaman, N. L.: Multiscale four-dimensional data assimilation, *J. Applied Meteorology*, 33, 416–434, 1994.
- Stavrakou, T., Müller, J. -F., Boersma, K. F., De Smedt, I., and van der A, R. J.: Assessing the distribution and growth rates of NO<sub>x</sub> emission sources by inverting a 10-year record of NO<sub>2</sub> satellite columns, *Geophys. Res. Lett.*, 35, L10801, doi:10.1029/2008GL033521, 2008.
- Stavrakou, T., Müller, J.-F., Boersma, K. F., van der A, R. J., Kurokawa, J., Ohara, T., and Zhang, Q.: Key chemical NO<sub>x</sub> sink uncertainties and how they influence top-down emissions of nitrogen oxides, *Atmos. Chem. Phys.*, 13, 9057–9082, doi:10.5194/acp-13-9057-2013, 2013.
- Stemmler, K., Ammann, M., Donders, C., Kleffmann, J., and George, C.: Photosensitized reduction of nitrogen dioxide on humic acid as a source of nitrous acid, *Nature*, 440, 195–198, doi:10.1038/nature04603, 2006.
- Streets, D. G., Bond, T. C., Carmichael, G. R., Fernandes, S. D., Fu, Q., He, D., Klimont, Z., Nelson, S. M., Tsai, N. Y., Wang, M. Q., Woo, J. -H., and Yarber, K. F.: An inventory of gaseous and primary aerosol emissions in Asia in the year 2000, *J. Geophys. Res.*, 108, 8809, doi:10.1029/2002JD003093, 2003.
- Svensson, R., Ljungström, E., and Lindqvist, O.: Kinetics of the reaction between nitrogen dioxide and water vapour, *Atmos. Environ.*, 21, 1529–1539, 1987.
- Tie, X., Emmons, L., Horowitz, L., Brasseur, G., Ridley, B., Atlas, E., Stroud, C., Hess, P., Klonecki, A., Madronich, S., Talbot, R., and Dibb, J.: Effect of sulfate aerosol on tropospheric NO<sub>x</sub> and ozone budgets: Model simulations and TOPSE evidence, *J. Geophys. Res.*, 108, 8364, doi:10.1029/2001JD001508, 2003.
- Uno, I., He, Y., Ohara, T., Yamaji, K., Kurokawa, J.-I., Katayama, M., Wang, Z., Noguchi, K., Hayashida, S., Richter, A., and Burrows, J. P.: Systematic analysis of interannual and seasonal variations of model-simulated tropospheric NO<sub>2</sub> in Asia and compar-

- ison with GOME-satellite data, *Atmos. Chem. Phys.*, 7, 1671–1681, doi:10.5194/acp-7-1671-2007, 2007.
- van der A, R. J., Peters, D. H. M. U., Eskes, H., Boersma, K. F., Van Roozendaal, M., De Smedt, I., and Kelder, H. M., Detection of the trend and seasonal variation in tropospheric NO<sub>2</sub> over China, *J. Geophys. Res.*, 111, 27, doi:10.1029/2005JD006594, 2006.
- Wang, Y., McElory, M. B., Martin, R. V., Streets, D. G., Zhang, Q., and Fu, T.-M.: Seasonal variability of NO<sub>x</sub> emissions over east China constrained by satellite observations: Implications for combustion and microbial sources, *J. Geophys. Res.*, 112, D06301, doi:10.1029/2006JD007538, 2007.
- Wild, O., Prather, M. J., and Akimoto, H.: Indirect long-term global radiative cooling from NO<sub>x</sub> emissions, *Geophys. Res. Lett.*, 28, 1719–1722, 2001.
- Willmott, C. J.: On the validation of models, *Phys. Geogr.*, 2, 184–194, 1981.
- Xing, J., Wang, S. X., Chatani, S., Zhang, C. Y., Wei, W., Hao, J. M., Klimont, Z., Cofala, J., and Amann, M.: Projections of air pollutant emissions and its impacts on regional air quality in China in 2020, *Atmos. Chem. Phys.*, 11, 3119–3136, doi:10.5194/acp-11-3119-2011, 2011.
- Yamartino, R. J.: Nonnegative, conserved scalar transport using grid-cell-centered, spectrally constrained Blackman cubics for applications on a variable-thickness mesh, *Mon. Weather Rev.*, 121, 753–763, 1993.
- Zhang, Q., Streets, D. G., He, K., Wang, Y., Richter, A., Burrows, J. P., Uno, I., Jang, C. J., Chen, D., Yao, Z., and Lei, Y.: NO<sub>x</sub> emission trends for China, 1995–2004: The view from the ground and the view from space, *J. Geophys. Res.*, 112, D22306, doi:10.1029/2007JD008684, 2007.
- Zhang, Q., Streets, D. G., Carmichael, G. R., He, K. B., Huo, H., Kannari, A., Klimont, Z., Park, I. S., Reddy, S., Fu, J. S., Chen, D., Duan, L., Lei, Y., Wang, L. T., and Yao, Z. L.: Asian emissions in 2006 for the NASA INTEX-B mission, *Atmos. Chem. Phys.*, 9, 5131–5153, doi:10.5194/acp-9-5131-2009, 2009.
- Zhou, X., Zhang, N., TerAvest, M., Tang, D., Hou, J., Bertman, S., Alaghmand, M., Shepson, P. B., Carroll, M. A., Griffith, S., Dusanter, S., and Stevens, P. S.: Nitric acid photolysis on forest canopy surface as a source for tropospheric nitrous acid, *Nat. Geosci.*, 4, 440–443, doi:10.1038/ngeo1164, 2011.
- Zyrichidou, I., Koukouli, M. E., Balis, D. S., Kioutsioukis, I., Poupkou, A., Katragkou, E., Melas, D., Boersma, K. F., and van Roozendaal, M.: Evaluation of high resolution simulated and OMI retrieved tropospheric NO<sub>2</sub> column densities over South-eastern Europe, *Atmos. Res.*, 122, 55–65, 2013.